

# Zoom $\oplus$ is what you need: An empirical study of the power of zoom and spatial biases in image classification

Mohammad Reza Taesiri \*

mtaesiri@gmail.com

Giang Nguyen <sup>†</sup>

nguyengiangbkhn@gmail.com

Sarra Habchi <sup>§</sup>

sarra.habchi@ubisoft.com

Cor-Paul Bezemer \*

bezemer@ualberta.ca

Anh Nguyen <sup>†</sup>

anh.ng8@gmail.com

\*University of Alberta

<sup>†</sup>Auburn University

<sup>§</sup>Ubisoft

## Abstract

Image classifiers are information-discarding machines, by design. Yet, how these models discard information remains mysterious. We hypothesize that one way for image classifiers to reach high accuracy is to first zoom to the most discriminative region in the image and then extract features from there to predict image labels. We study six popular networks ranging from AlexNet to CLIP and find that proper framing of the input image can lead to the correct classification of 98.91% of ImageNet images. Furthermore, we explore the potential and limits of zoom transforms in image classification and uncover positional biases in various datasets, especially a strong center bias in two popular datasets: ImageNet-A and ObjectNet. Finally, leveraging our insights into the potential of zoom, we propose a state-of-the-art test-time augmentation (TTA) technique that improves classification accuracy by forcing models to explicitly perform zoom-in operations before making predictions. Our method is more interpretable, accurate, and faster than MEMO, a state-of-the-art TTA method. Additionally, we propose ImageNet-Hard, a new benchmark where zooming in alone often does not help state-of-the-art models better label images.

## 1. Introduction

Since the release of AlexNet in 2012 [31], image classifiers have set many ImageNet (IN) [48] classification accuracy records [20, 31]. While many papers reported improved learning algorithms or architectures, little is known about how the inner workings of image classifiers actually evolve. The success is often attributed to a network’s ability to detect more objects [8] and a variety of facets of each object [18, 42]. From all the objects and visual cues detected

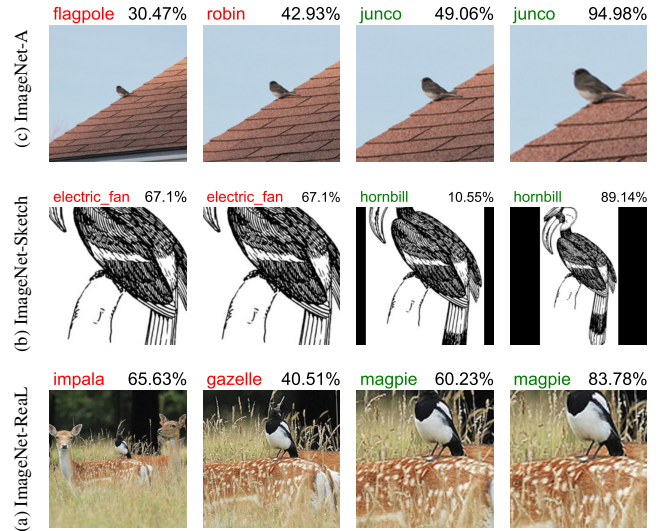


Figure 1: Each subfigure shows an input image, predicted label, and confidence score from an ImageNet model (top and middle: ResNet-50 [20]; bottom: ViT-B/32 [14]). With the standard center-crop image transform, all 3 samples were **misclassified** (left-most column). Adjusting the framing by zooming in or out leads to **correct** predictions.

in a scene, modern models would be able to choose a better label from the entire image. For example, Figs. 13–14 in [47] show that a model detects both dogs and cats in the same image and only discards the dog features right before the classification layer to arrive at a `tiger cat` prediction.

We pose an alternative, non-mutually-exclusive hypothesis: A model first *zooms* (defined in Sec. 3) in or out to the most salient region in an image *ignoring* the rest of the image (Fig. 1), and then extracts that localized region’s fea-

tures to predict image labels. That is, we hypothesize that the improved image classification also be due to a modern network accurately zooms to the *junco* and *maggie* birds in Fig. 1 rather than more accurately describing them (*i.e.* generating better features). In this work, we present supporting evidence for our hypothesis.

In particular, via a rigorous study across six well-known network architectures and six ImageNet-scale benchmarks, we show that **state-of-the-art IN-trained models can accurately predict up to 98.91% of ImageNet samples when an optimally-zoomed image is provided** (Sec. 4.1). The remaining few hundred IN images (0.39%) that are never correctly labeled by any model (despite optimal zooming) include mostly *ill-posed* and *rare* images (Sec. 4.1), which are similar to the adversarial images of ObjectNet [7] and ImageNet-A [24].

In addition, we make the following observations w.r.t. zooming on the studied architectures and benchmarks:

- ImageNet-A and ObjectNet both contain a large center bias, *e.g.* simply upsampling and then center-cropping every ImageNet-A image will boost the accuracy of ResNet-50 from 0.09% to 14.58% (Sec. 4.4).
- Zooming in or out can help IN-trained networks on ImageNet-A and ObjectNet but hurts CLIP’s [44] accuracy, suggesting that CLIP may internally perform implicit zooming (Sec. 4.5).
- In practice, when the optimal zooming procedure is unknown, aggregating the prediction results over multiple pre-defined zoom-in versions of the input can yield **better** accuracy than the standard 1-crop and 10-crop evaluation on several datasets (Sec. 4.6).
- Incorporating zoom transformations into MEMO [69], a state-of-the-art test-time augmentation technique, leads to consistently superior accuracy compared to the baseline ResNet-50 models and even better accuracy than MEMO (with its default transformations) on multiple datasets (Sec. 4.7).
- We introduce ImageNet-Hard, a collection of images derived from various ImageNet validation sets that remain unclassifiable despite the use of zoom techniques. (Sec. 4.8)

## 2. Related Work

**Learning to Zoom in image classification** Zooming in provides more details and has been useful in image classification [15, 27, 30, 45, 58, 61]. When zooming inside an image, details (*e.g.* textures) become more visible to a classifier, and background clutters can be eliminated. Importantly, Li et al. [35] showed that the performance of several models on the challenging ImageNet-A [24] dataset can be improved by only cropping out the image’s primary object. Furthermore, to our knowledge, zooming out (viewing from afar) is less studied and has never been visited in the image

classification context. These two motivate us to investigate the extent to which zoom, as the sole factor, can improve the accuracy of image classification.

**Test-time data augmentation (TTA)** is a versatile technique that could help estimate uncertainty [5, 6, 54] and improve classification accuracy [13, 20, 28, 31, 38, 43, 51, 57]. When test inputs are sampled from unseen, non-training distributions, augmenting the data often improves a model’s generalization to new domains [62, 69].

A simple TTA method is 10-crop evaluation [31] in which 5 patches of  $224 \times 224$  px along with their horizontal reflections (resulting in 10 patches) are extracted from the original image. The final prediction is obtained by averaging the outputs of the model over these patches. Other crop-based variants [20, 52, 57] were also invented to improve accuracy. These multi-crop augmentations serve as baselines for our evaluation in Sec. 4.6.

Regarding prediction aggregation, some approaches prioritize certain augmentations over others. For example, one can develop an aggregator that assigns different weights to each augmented input [13, 28, 51]. Like previous studies [38, 50], we report the performance of the naive mean and max aggregation operations, which surprisingly can achieve improved accuracy (Tab. 4)

An alternative way to leverage the marginal output distributions over augmented data is to use them as gradient signals to update the classifier’s parameters [63, 69]. This aggregation approach makes fewer assumptions about model architecture or training process, unlike [56, 70]. We employ this approach to update the model during test time, with patches being zoom-based augmentations.

**Biases in ImageNet and datasets** Resizing-then-cropping at the center has been a pre-processing standard for image classification since AlexNet [31]. This pre-processing exploits the known center bias of ImageNet. While other ImageNet biases have been documented: annotation [9, 60], object pose & professional photography [32], or biodiversity [37], we are the first to examine the positional biases of the OOD benchmarks for ImageNet classifiers and find a strong center bias in ImageNet-A and ObjectNet that could affect how the community perceives progress on these OOD benchmarks.

## 3. Method

**Zoom definition** To zoom in or out of the image, we rely on the combination of simple *resize* and *crop* operations. Initially, we uniformly resize the test image so that the smaller dimension matches the target scale of  $S$ . Then, we define a grid on the image to divide it into 9 ( $3 \times 3$ ) patches. We perform a *CenterCrop* operation at the center of each patch to extract a  $224 \times 224$  px crop from each of the nine locations (sample code is provided in Appendix A.1). In the *CenterCrop* step, *zero padding* will be added to a

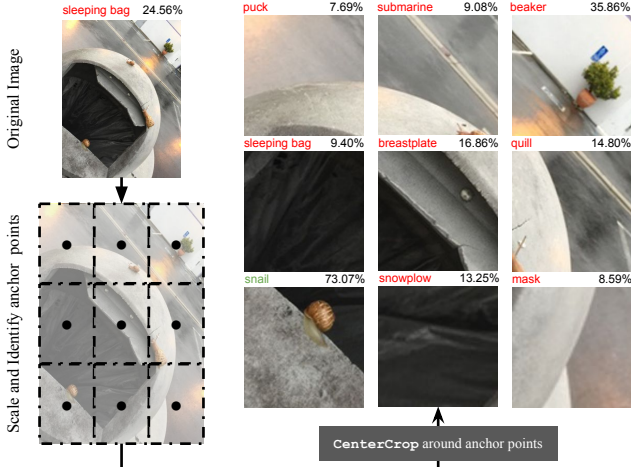


Figure 2: The zooming process leads to the correct classification of a *snail* image from ImageNet-A. We uniformly scale the input query image up or down so that the smaller dimension matches a target scale  $S$ . Next, we divide the image into a  $3 \times 3$  grid and generate 9 crops centered at the grid-cell’s centers (*i.e.* anchor points).

patch, ensuring its final size. Fig. 2 demonstrates how a ResNet-50, in which the shown image is misclassified as a *sleeping bag* using the standard ImageNet transform, can correctly classify the image as a *snail* using the zoom-in process.

We test a total of 36 different values of  $S$  ranging from 10 to 1024 px, resulting in a total of  $36 \times 9 = 324$  different augmented versions for each image. Based on initial scale factor  $S$ , we define three groups: The *zoom-out* group contains all augmented images where  $S < 224$ ; the *zoom-in* group contains all augmented images where  $S > 224$ ; and the *zoom-224* group contains the 9 patches where  $S = 224$ .

**Benchmark datasets** We use the ImageNet (IN) [48] dataset with both the original and ImageNet-Real [9] (ReaL) labels. For each IN image, we use the union of the IN and ReaL labels (IN+ReaL) to complement each other to reduce noise in IN labels. We further examine the effects of zoom-based transformations on four popular out-of-distribution (OOD) benchmarks: (a) natural adversarials (ImageNet-A [24]), (b) image renditions (ImageNet-R [21]), (c) black-and-white sketches (ImageNet-Sketch [63]), and (d) viewpoint-and-background-controlled samples (ObjectNet [7]). We refer to these as benchmarks as IN-A, IN-R, IN-S, and ON, respectively, in the rest of the paper.

**Classifiers** We study the effects of zoom-based transformations on six image classifiers: ResNet-18 & ResNet-50 [20], ViT-B/32 [14], VGG-16 [52], AlexNet [31], and CLIP-ViT-L/14 [44]. The inclusion of the 10-year-old AlexNet provides a baseline for the power of representa-

tions if we harness them properly (*i.e.* by giving AlexNet the right region to look at). We include CLIP-ViT-L/14 as a state-of-the-art representative in our study as well to compare multimodal vs. conventional, unimodal image classifiers. Predicted labels from CLIP are acquired using its standard zero-shot classification setup (Appendix A.4).

## 4. Experimental Results

In this section, we present six experiments to explore the effectiveness of zooming transforms in image classification. First, we examine the upper limits of zoom potential in Sec. 4.1 and explore how the bias in different datasets affects the number of zoom transforms needed to achieve upper limits in Sec. 4.2. In Sec. 4.3 we show which zoom group is the most beneficial. In Sec. 4.4, we use zoom transforms to demonstrate center bias in some popular datasets. We study CLIP’s inherent power to perform zoom and contrast it with other models in Section 4.5. Next, we show the limits of simple aggregation in Section 4.6 and demonstrate how to directly promote implicit zooming during inference in Section 4.7. Finally, we introduce the ImageNet-Hard dataset in Sec. 4.8, which is a collection of images that remain unclassifiable using various zoom transforms.

### 4.1. Zoom has the potential to substantially improve image classification accuracy

To understand the potential of using zooming to improve image classification accuracy, first, we establish an upper bound (*i.e.* when an “optimal” zoom is given). That is, we apply  $36 \text{ scales} \times 9 \text{ anchors} = 324$  zoom transformations (Sec. 3) to each image to generate 324 zoomed versions of the same input. We then feed all 324 versions to each network and label an image “correctly classified given the optimal zoom” if at least 1 of the 324 is correctly labeled.

This experiment also importantly informs the community of the type of image that *cannot* be correctly labeled even with an optimal zooming strategy.

**Results** Table 1 shows the top-1 accuracy and maximum possible accuracy values of our experiment. First, the **random** baselines (given  $N = 324$  attempts per image) are at 32.4% for 1,000 classes (IN, ReaL, IN+ReaL, and IN-Sketch), and 100% for 200 and 313 classes (IN-A and ON, respectively). Yet, the accuracy of models with optimal zooming is far from random—*e.g.* ResNet-50 substantially outperforms not only the random baseline but also the 1-crop baseline on IN (96.78% vs. 75.75%; Tab. 1a vs. c).

On the IN, ReaL, and IN+ReaL datasets, there is a substantial gap for all models (around +20 to +35 points) between the 1-crop and the optimal zooming setting (Tab. 1a vs. c). Surprisingly, given optimal zooming, the 10-year-old AlexNet actually can correctly label  $\geq 90\%$  of IN images, which is roughly the 1-crop accuracy of the 2022 state-of-the-art ConvNexts (87.8%) [36]. This result is consistent



Table 1: On in-distribution data (IN & ReaL) there exists a substantial improvement when models are provided with an optimal zoom, either selected from 36 (b) or 324 pre-defined zoom crops (c). In contrast, OOD benchmarks still pose a significant challenge to optimal zooming as none of the models (except CLIP) can reach  $\geq 80\%$  accuracy.

	IN	ReaL	IN+ReaL	IN-A	IN-R	IN-S	ON
(a) Standard top-1 accuracy based on $N = 1$ crop							
ResNet-18	69.45	76.94	76.47	1.37	32.14	19.41	27.59
ResNet-50	75.75	82.63	82.97	0.21	35.39	22.91	36.18
ViT-B/32	75.75	81.89	82.59	9.64	41.29	26.83	30.89
VGG-16	71.37	78.90	78.52	2.69	26.98	16.78	28.32
AlexNet	56.16	62.67	61.76	1.75	21.10	10.05	14.23
CLIP-ViT-L/14	75.03	80.68	81.95	71.28	87.74	58.23	66.32
(b) Maximum possible accuracy using $N = 36$ crops							
Random	3.60	3.60	3.60	18.00	3.60	3.60	31.85
ResNet-18	92.08	95.97	95.73	58.85	47.48	37.91	63.08
ResNet-50	94.46	97.36	97.40	61.42	55.68	41.71	69.60
ViT-B/32	95.05	97.61	97.88	68.77	68.43	49.10	70.30
VGG-16	92.30	96.08	95.81	52.86	46.69	34.34	62.94
AlexNet	85.19	90.30	89.74	47.04	31.37	24.40	49.17
CLIP-ViT-L/14	94.19	97.32	97.56	98.60	97.16	83.77	89.59
(c) Maximum possible accuracy using $N = 324$ crops							
Random	32.40	32.40	32.40	100.00	100.00	32.40	100.00
ResNet-18	95.15	97.76	97.55	58.87	66.89	43.68	71.44
ResNet-50	96.78	98.62	98.57	66.68	68.84	47.64	76.83
ViT-B/32	<b>97.19</b>	<b>98.75</b>	<b>98.91</b>	78.03	75.58	55.99	79.28
VGG-16	95.30	97.90	97.66	58.27	60.88	39.90	71.85
AlexNet	90.03	93.85	93.48	42.23	55.52	29.53	59.65
CLIP-ViT-L/14	96.78	98.69	98.80	<b>98.45</b>	<b>99.20</b>	<b>89.00</b>	<b>93.13</b>

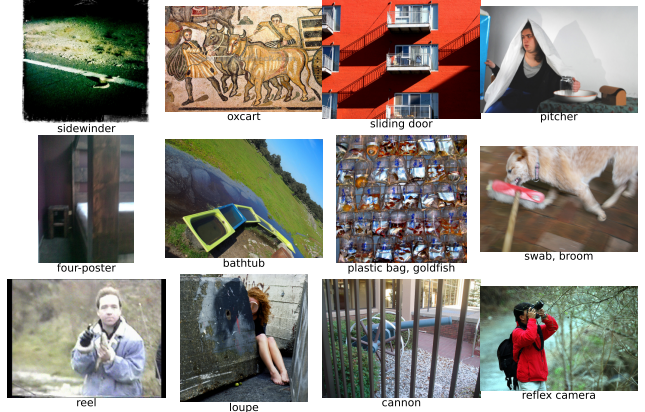
with our hypothesis: One way for state-of-the-art classifiers to obtain their current accuracy is to simply learn how to zoom on top of the same, old feature extractors (e.g. that of AlexNet).

**Unclassifiable IN images** Interestingly, even with optimal zooming, no model ever reaches 100% on IN images. We find that 0.39% of the IN+ReaL images were not classified correctly by any of the IN-trained classifiers and that these images are similar to natural adversarial images (Fig. 3) and can be categorized into four groups:

- Lack of information: Images do not contain sufficient signals for classification, i.e. low lighting, occlusion, or low-quality photos (Fig. 3a).
- Rare cases: Images show the main object but in an unusual rendition, pose, or form (Fig. 3b).
- Illusions: Images contain fooling elements or artifacts, e.g. a shadow that looks like a staircase, causing the misclassification (Fig. 3c).
- Many objects: Multiple classes of objects appear in a single image but the ground-truth labels do not cover all classes (Fig. 3d).

**OOD datasets pose a significant challenge to IN-trained models despite optimal zooming.** Across all OOD datasets, all IN-trained models perform far below the random baseline (100%) with the highest score being 79.28%

(Tab. 1). Our result suggests that OOD images (e.g. objects in unusual poses or renditions) require a more robust fea-



(a) Lack of info (b) Rare cases (c) Illusions (d) Many objects

Figure 3: All sample images from the IN+ReaL, that are not classifiable by IN-trained networks using any zoom transforms.

ture extractor to recognize besides zooming. Aligned with our conjecture above, CLIP reaches extremely high scores upon optimal zooming (98.45% on IN-A and 99.20% on IN-R; Tab. 1). An explanation is that CLIP was trained on a large-scale web dataset [44] and thus is robust to pose, style, and shape changes of objects [18].

## 4.2. Only 70% of all transforms are needed to reach maximum possible accuracy

In Sec. 4.1, we first pre-define all 324 zoom transforms and then compute the *maximum* possible accuracy to ensure the predicted labels were the results of models looking at a controlled zoomed region (i.e. not because a model was given 324 arbitrary trials per image). Here, we aim to compute the minimum number of zoom settings required for a model to reach the same upper-bound accuracy. Evaluating this minimum set may reveal spatial biases of a dataset (Sec. 4.4) as well as the implicit zoom operation that a state-of-the-art model (e.g. CLIP) may have learned.

**Experiment** Given a (dataset, classifier) pair, each zoom transform among the 324 will result in a set of correctly classified images. We employ a greedy minimum-set cover algorithm [29, 53] to find a minimum subset of transforms that lead to the correct prediction for all classifiable images in Sec. 4 (i.e. those that make up the accuracy scores in Tab. 1c).

For each dataset and classifier pair, we construct a bipartite graph, consisting of transforms and images as distinct groups of nodes. We connect a node from the transform group to an image node, if that transform leads to the correct classification of that particular image. Finding a minimum set cover in this graph is the same as finding the afore-



Table 2: The minimum number of zoom transforms (out of 324) required to achieve the maximum possible accuracy scores reported in Tab. 1c.

	IN	ReaL	IN+ReaL	IN-A	IN-R	IN-S	ON	$\mu$
ResNet-18	250	201	208	211	278	269	254	239
ResNet-50	234	178	183	214	271	281	259	231
ViT-B/32	233	168	173	193	257	273	273	224
VGG-16	242	201	201	222	289	273	259	241
AlexNet	255	239	246	212	272	275	268	252
CLIP-ViT-L/14	251	197	186	93	114	280	212	190

mentioned subset of transforms. During each iteration of the greedy minimum set cover algorithm, the transform that yields the highest number of correct classifications for the remaining images is selected. This process continues until all of the images have been “covered”, *i.e.* all images have connected to a transform with at least one edge. The result is a subset of transforms that can classify images without sacrificing accuracy.

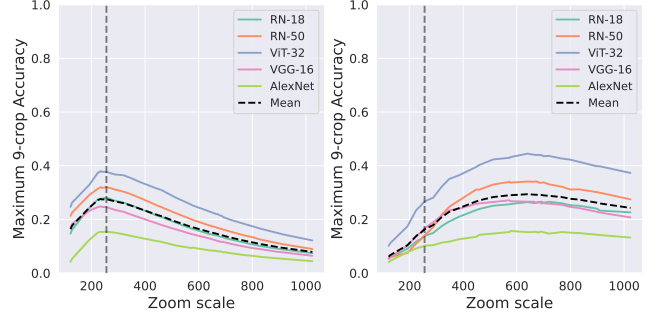
**Results** Tab. 2 shows the minimum number of transforms per dataset required to reach the maximum possible accuracy. Although this number varies depending on the dataset and classifier, on average, the size of the minimum cover is 229, which is  $\sim 70\%$  of all 324 pre-defined transforms.

We evaluate the maximum possible accuracy using the top 36 transforms, the same number as the number of zoom scales, and report the results in Tab. 1b. This set of transforms is achieved by stopping the algorithm after 36 iterations, which provided us with 36 high-performing transforms. The maximum possible accuracy using only 36 crops is only slightly lower than that when using all 324 crops but is substantially higher than the standard 1-crop, *e.g.* 85.19% vs. 56.16% for AlexNet on IN (Tab. 1b). Also, the upper-bound accuracy for 36 crops being much higher than the random baseline (*i.e.* 3.6% for IN) confirms that the pre-defined zoom transforms are important to classification (not because models are given 36 random trials per image). The top-36 zoom transforms for ResNet-50 on ImageNet contain zooms at various locations in the image (see the visualizations in Appendix D.1).

Remarkably, CLIP requires 190 transforms on average, which is fewer than every other model (Tab. 2;  $\mu$  column). This can be attributed to either the implicit zoom power of CLIP or the fact it has a stronger feature extractor.

#### 4.3. Zoom-in is more useful than zoom-out, which is most important to abstract images

Zooming in enhances texture patterns while zooming out provides a better perspective of the object’s shape, which is known to be useful to image classification [11, 17]. Results in Secs. 4.1 and 4.2 indicate that this combined zooming approach can be effective in classifying images from diverse datasets. Here, we test which dataset and model pairs re-



(a) ImageNet-Sketch

(b) ImageNet-A

Figure 4: Maximum possible accuracy using nine crops at varying scales. The vertical line represents the standard ImageNet zoom scale ( $S = 256$ ). While for ImageNet-Sketch (a), zooming out marginally improves the accuracy, for scale factors larger than 256, ImageNet-A (b) exhibits an increase in accuracy. See Appendix B.6 for details.

quire which type of zoom, and whether zooming in or out is always necessary.

**Experiment** To better understand the effectiveness of each zoom group, we calculate the maximum possible accuracy using all nine locations and different zoom scales  $S$  to show per-dataset trends. Additionally, we examined the percentage of images within each dataset that required a specific zoom group to be accurately classified. This analysis allowed us to gain a more comprehensive understanding of the role that each zoom group played in reaching the maximum possible accuracy reported in Tab. 1.

**Results** The maximum possible accuracy for different zoom scales reveals a clear trend for each dataset. For instance, for datasets that contain abstract images such as ImageNet-Sketch, a slight zoom-out boosts accuracy (Fig. 4a). In contrast, for datasets that include adversarial images like ImageNet-A, zoom in improves accuracy (Fig. 4b). We also observed this pattern when evaluating models using standard 1-crop accuracy (Appendix B.6).

Furthermore, the percentage of images that are *exclusively* classifiable with the *zoom-in* group is consistently higher than the other two groups, *i.e.* using ViT-B/32 51.75% on IN-A, and 13.11% on IN-S (Tab. 3a). This shows that most datasets necessitate focusing on the object of interest in the image to both see texture patterns better and reduce background clutter (see Tab. A1 for full results).

However, we also find that the *zoom-out* group is also necessary for the correct classification of a small portion of each dataset. For instance, 1.22% – 2.97% of IN-S images (Tab. 3b) require a *zoom-out* transform to be correctly labeled (*i.e.* *zoom-in* does not help at all).

Table 3: % of images in the entire dataset that requires a particular zoom group to be classified correctly. See Tab. A1 for full results.

	<i>zoom-in</i> (a)		<i>zoom-out</i> (b)		<i>zoom-224</i> (d)	
	IN-A	IN-S	IN-A	IN-S	IN-A	IN-S
ResNet-18	40.67	11.83	0.92	1.77	0.19	0.36
ResNet-50	48.72	10.99	1.00	2.23	0.23	0.24
ViT-B/32	51.75	13.11	0.85	1.83	0.15	0.36
VGG-16	38.24	9.47	0.93	2.97	0.29	0.28
AlexNet	26.27	11.26	1.08	1.22	0.36	0.33
CLIP-ViT-L/14	12.01	6.64	0.44	2.38	0.05	0.12

#### 4.4. ImageNet-A and ObjectNet suffer from a severe center bias

A standard image pre-processing transform for IN-trained models is to first resize the image such that its smaller dimension is 256 and then take the center  $224 \times 224$  crop of the resized image as the pre-processed image [1, 31]. While this pre-processing is suitable for ImageNet (which is center-biased), it may not be optimal for every OOD dataset as it does not allow a model to fully utilize the off-center visual cues near the edges of an image (which optimal zooming would allow). Leveraging the minimum zoom set obtained in Sec. 4.2, we quantify which spatial locations (out of 9 anchors; Fig. 2) contain the most discriminative features in each dataset. That is, we compute the upper-bound accuracy for each of the 9 spatial zoom locations per dataset and discover surprising biases in some existing benchmarks.

**Experiment** For each image, we have 9 anchors (Fig. 2) and the originally  $K = 36$  zoomed versions per anchor as defined in Sec. 3. Yet, after reducing to the minimum set (Sec. 4.2),  $k$  averages at 25, over all datasets, and  $10 \leq k \leq 31$ . Here, we count the percentage of times that the  $K$  zoomed versions per anchor lead to a correct prediction. In other words, we compute the maximum possible accuracy as in Sec. 4.1 but for each anchor separately.

**Results** First, as expected, the upper-bound accuracy for each anchor (Fig. 5) is consistently lower than when all 9 anchors are allowed (Tab. 1c).

Second, across all 6 datasets, the center anchor consistently reaches the highest upper-bound accuracy compared to the other 8 locations (Fig. 5 and Appendix B.3), showing that all datasets contain a center bias. However, we find the center bias is fairly small in IN, IN-R, and IN-S but extremely large in ImageNet-A and ObjectNet (*i.e.* the largest difference between the center accuracy and the lowest off-center accuracy is -23 and -25 points, respectively; Fig. 5).

The center bias in ObjectNet can be explained by the fact that the images were captured using smartphones with aspect ratios of 2:3 or 9:16 (Appendix D.3.3). Overall, such strong center bias in ImageNet-A and ObjectNet may not

46.81	47.96	46.85	21.17	26.77	21.59	57.55	60.28	57.59
62.25	69.30	62.53	27.57	46.49	26.57	59.49	62.52	59.62
48.42	49.84	48.55	22.52	27.61	22.31	57.09	59.60	57.19

(a) ObjectNet      (b) ImageNet-A      (c) ImageNet-R

Figure 5: Maximum possible top-1 accuracy (%) of ResNet-50 at each of the 9 zoom locations. The large accuracy gaps between the center and eight off-center locations on ImageNet-A and ObjectNet demonstrate the presence of a center bias. The bias is much smaller in ImageNet and ImageNet-R (c). See Appendix B.3 for more results.

be desirable since improvements on these two benchmarks may be attributed to learning to zoom to the center as opposed to the intended quest of recognizing objects in unusual forms (IN-A) or poses (ON). By merely upscaling the image and center cropping, we can achieve higher accuracy using nearly all models on these two datasets (Figs. A11 and A14).

#### 4.5. Center-zooming increases the accuracy of all ImageNet-trained models but not CLIP

Previously, we have found that CLIP obtains the best accuracy on all six datasets (Tab. 1a) and also requires the smallest minimum set of zoom transforms to obtain the upper-bound accuracy (Sec. 4.2). It is important to understand what classification strategy a CLIP classifier internally performs to classify better. Here, we test the hypothesis that the state-of-the-art CLIP is already performing an implicit zoom on images. If that is true, directly zooming to the center, exploiting the strong center bias of ImageNet-A and ObjectNet, will not improve CLIP accuracy.

**Experiment** We evaluate the accuracy of all models when center-zooming on IN-A and ON images at 11 different scales  $S \in \{128, 160, 192, \dots, 448\}$  (Fig. 6). That is, center-zooming at  $S$  first resizes the input image so that the smaller dimension becomes  $S$  and then takes a  $224 \times 224$  center crop (zero-padding is applied when necessary).

**Results** In Fig. 6, we show the changes in the top-1 accuracy (1-crop) when varying the center-zoom scales away from the default ImageNet transform scale ( $S = 256$ ) for both ImageNet-A and ObjectNet. While IN-trained networks exhibit consistent improvement as the zoom scale increases, CLIP shows a monotonic decrease in performance (Fig. 6; yellow curves decreasing on both sides of  $S = 256$ ). This result is surprising but consistent with our hypothesis that CLIP internally performs implicit zooming to reach its peak accuracy and therefore manually zooming (either in or out) at the center mostly ruins its performance.

The fact that CLIP does not benefit from center-zooming

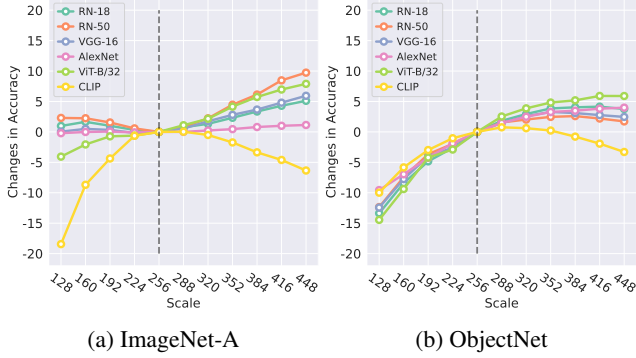


Figure 6: Absolute changes in the top-1 accuracy (%) of 6 models on ImageNet-A (a) and ObjectNet (b) when center-zooming images at various scales. Interestingly, center-zooming helps IN-trained networks but hurts CLIP.

on IN-A and ON images is even more interesting provided that the images in these two datasets often contain even more distracting objects than ImageNet images (statistics in Appendix C.2) and therefore, center-zooming *should* help de-clutter the scene for more accurate classification. That is, CLIP appears to strongly prefer a specific zoom scale that enables sufficient background to recognize objects—it was also found to perform poorly in identifying a single object placed in a tightly-cropped image [71]. Future research should further investigate whether this “zoom bias” of CLIP reported here is due to its image- or text-encoder or both.

#### 4.6. Simple aggregation of the zoom transforms can improve accuracy on some datasets but not all

Secs. 4.1 and 4.5 show that using the same feature extractors (even as old as AlexNet), it is possible to achieve higher image classification accuracy if we know where to zoom and at which scale. A practical follow-up question is: How to build a classifier that knows how to zoom given a test image? In this section, we establish simple baselines that aggregate predictions over a set of zoom transforms.

**Experiment** We employ the mean method from prior work [38, 50], and the max method to aggregate output marginal distributions. For a given image, we get  $N$  output distributions over classes from a classifier, in which  $N$  is the total number of used transforms. The aggregation process combines these  $N$  distributions and outputs a final prediction for the given image. In the aggregation step, we use the mean or max method to infer the final confidence for each class along  $N$  distributions. Finally, we select the class that has the highest confidence score. Additionally, we test 5-crop and 10-crop evaluation [20, 31, 52] and compare them with our methods. We use the transforms in the minimum set found for IN-ReaL to evaluate the remaining datasets. The purpose is to reduce the number of augmentations and

prevent training on OOD benchmarks.

**Results** max aggregation of zoom-in transforms results in the largest improvements on ImageNet-A. That is, on IN-A, ViT-B/32 reaches a top-1 accuracy of 24.69% (+15.05) (Tabs. 4 and A2) and a ResNet-50 accuracy increases by +13.03 points from 16.62% to 29.65% (Appendix C.3)—a surprisingly strong baseline for future studies. On ObjectNet, max aggregation of zoom-in transforms also yields +1.99 improvement over the 1-crop ViT-B/32 baseline.

On the other hand, mean aggregation results in smaller but more consistent improvements over the 1-crop baseline for many datasets (+3.56 on IN, +4.08 on ReaL, +4.65 on IN-A, and +3.03 on ON; Tab. 4). mean aggregation (Tab. 4b) also outperforms the standard 5-crop and 10-crop [20, 31] aggregation on these four datasets (Tab. 4e–f).

In contrast, for all 6 datasets, aggregating zoom-out and zoom-224 transforms consistently worsen the performance over the 1-crop baseline (Tab. 4c–d). That is, we find that for a few dozen images (e.g. sketches and abstract visuals; Fig. 1c), interestingly, only zooming out can lead to a correct classification (Sec. 4.3), yet for most images in these 6 benchmarks, zooming out hurts the accuracy.

In summary, based on the insights from Sec. 4.1, showing that zooming could help classification, we find that simple methods for aggregating zoom-in transforms at test-time can directly improve model accuracy over the 1-crop and zoom-224 baselines on four benchmarks, *i.e.* all except IN-R and IN-S, which contain abstract images.

#### 4.7. Test-time augmentation of MEMO with only zoom-in transforms improves accuracy

State-of-the-art test-time augmentation methods, such as MEMO [69], finetune a pre-trained classifier at *test* time to achieve a more accurate prediction. Specifically, MEMO attempts to find a network that produces a low-entropy predicted label over a set of  $K = 16$  augmented versions of the test image  $I$  and then runs this finetuned model on  $I$  again to produce the final prediction. While improving accuracy, MEMO requires a pre-defined set of diverse augmentation transforms (e.g. shear, rotate, and solarize in AugMix [21]). Yet, the hyperparameters for each type of transform are hard-coded, and the reasons why some of such transform help classification are unknown.

Our goal is to improve MEMO’s accuracy and interpretability by replacing all AugMix transforms with only zoom-in transforms. Intuitively, we let a classifier first look at all zoomed-in frames of the input image (at different zoom scales and locations) and then make up its mind to achieve the most confident prediction.

**Experiment** MEMO relies on AugMix [23] to produce augmentations of the input image. AugMix applies a set of 13 image transforms, such as translation, rotation, and color distortion, to an original image at varying intensities, and



Table 4: Top-1 accuracy (%) of aggregation methods on an IN-trained ViT-B/32 model. Compared to the 1-crop baseline, aggregating zoom-in transforms consistently yields **improved** accuracy on IN-A, ON but **worse** accuracy on IN-R and IN-S. *zoom-224* refers to the set of zoom transforms at  $S = 224$ . See Tab. A2 for more results.

	(a)	(b) <i>zoom-in</i> $\oplus$		(c) <i>zoom-out</i> $\ominus$		(d) <i>zoom-224</i>		(e) 5-crop		(f) 10-crop [31]	
<b>Dataset</b>	1-crop	max	mean	max	mean	max	mean	max	mean	max	mean
IN	75.75	74.35 (-1.40)	<b>79.31</b> (+3.56)	71.48	69.47	72.66	73.67	77.33	77.73	77.30	77.87
ReaL	81.89	80.22 (-1.67)	<b>85.97</b> (+4.08)	77.95	76.28	79.25	80.31	83.24	83.80	83.17	83.87
IN-A	9.64	<b>24.69</b> (+15.05)	14.29 (+4.65)	7.79	5.48	8.12	7.39	12.19	9.88	12.32	9.67
IN-R	41.29	39.90 (-1.39)	40.06 (-1.23)	39.05	36.21	39.52	39.28	43.90	43.17	<b>44.31</b>	43.28
IN-S	26.83	19.74 (-7.09)	20.89 (-5.94)	22.37	19.25	25.06	25.21	28.72	28.66	<b>28.94</b>	28.76
ON	30.89	32.88 (+1.99)	<b>33.92</b> (+3.03)	22.56	19.51	22.75	22.72	26.96	24.98	27.14	24.97

then *chains* them together to create  $K = 16$  new augmented images (examples in Appendix D.5).

We replace AugMix by RandomResizedCrop [3] (RRC), which takes a random crop of the input image (*i.e.* at a random location, random rectangular area, and a random aspect ratio) and then resizes it to the fixed  $224 \times 224$  (*i.e.* the network input size). RRC basically implements a random zoom-in function (examples in Appendix D.5).

We compare the original MEMO [69] (which uses AugMix) and our version that uses RRC on IN and its four OOD benchmarks (IN-A, IN-R, IN-S, and ON). We follow the same experimental setup as in Zhang et al. [69] (*e.g.*  $K = 16$ ). Specifically, we test three ResNet-50 variants that were pre-trained using distinct augmentation techniques.<sup>1</sup>

**Results** Both our MEMO + RRC and the original MEMO + AugMix [69] consistently outperform the baseline models, which do not use MEMO, on all five datasets (Tab. 5). That is, when combined with MEMO, zoom-in transforms implemented via RRC are also helpful in classifying IN-S and IN-R images—where we previously found zoom-in to *not* help in mean/max aggregation (Sec. 4.6).

On average, over all three models and five datasets, our RRC outperforms AugMix by **+0.28** points, with a larger impact on ImageNet-A, where it achieves a mean improvement of **+1.10** points. Aligned with our prior sections, here, the results show that zoom-in alone can be a useful inductive bias, helping improve downstream image classification. In contrast, some of the transformations among the 13 transform functions in AugMix may not be essential to the result of Zhang et al. [69] (no ablation studies of transformations were provided in [69]) and are less effective than zoom-in.

**Speed-up** Another benefit of RRC compared to AugMix is faster inference time. Typically, TTA methods suffer from slow runtime due to augmentation and test-time training processes. We find that MEMO + RRC consistently leads to an average **1.6 $\times$**  speed-up compared to MEMO + AugMix (Tab. A4; 0.65s / image vs. 1.15s / image), providing more

Table 5: Overall, MEMO + RRC (*i.e.* random zoom-in transforms) **outperforms** baselines and the default MEMO.

Top-1 accuracy (%)	IN	IN-A	IN-R	IN-S	ON
Baseline (1-crop)					
ResNet-50 [20]	76.13	0.00	36.17	24.09	35.92
DeepAug+AugMix [21]	75.82	3.87	46.77	32.62	34.81
MoEx+CutMix [33]	79.04	7.97	35.52	23.96	38.59
<i>mean <math>\pm</math> std</i>		36.75 $\pm$ 24.75			
MEMO + AugMix [69]					
ResNet-50 [20]	77.27	0.83	<b>41.28</b>	<b>27.63</b>	38.38
DeepAug+AugMix [21]	76.27	5.35	50.79	<b>35.70</b>	36.42
MoEx+CutMix [33]	79.38	11.21	<b>40.65</b>	<b>27.07</b>	40.62
<i>mean <math>\pm</math> std</i>		39.26 (+2.51) $\pm$ 24.32			
MEMO + RRC (Ours)					
ResNet-50 [20]	<b>77.50</b>	<b>1.31</b>	40.81	27.53	<b>38.85</b>
DeepAug+AugMix [21]	<b>76.38</b>	<b>5.76</b>	<b>50.88</b>	35.65	<b>36.64</b>
MoEx+CutMix [33]	<b>79.49</b>	<b>13.61</b>	40.41	26.80	<b>41.43</b>
<i>mean <math>\pm</math> std</i>		<b>39.54</b> (+2.79) $\pm$ 24.10			

evidence to support this transformation as a viable option for test-time augmentations.

#### 4.8. ImageNet-Hard benchmark challenges models to classify images where zooming does not help

An existing ImageNet-scale OOD benchmark was often created based on one of the following three approaches: (1) modify the original in-distribution images into OOD images (*e.g.*, ImageNet-C [22] and DAmageNet [12]); (2) collect the real images that models misclassify (*e.g.*, ImageNet-A, ImageNet-O [24]); or (3) setting up highly-controlled data collection process (*e.g.*, images of sketches [63] or of objects in unusual poses [4, 7]). Yet, in all existing benchmarks, it is unclear whether misclassifications are due to failures to *localize* key objects in an image or to *recognize* already-localized objects (*e.g.* those in unusual poses [4]). To disentangle these two effects, we propose a novel ImageNet-Hard dataset where even zooming does *not* help

<sup>1</sup>The ResNet-50 model used as a baseline in this Sec. 4.7 is different from that in our other (non-MEMO) sections of the paper.

CLIP ViT-L/14 to correctly label the images. ImageNet-Hard serves as a hard, ImageNet-scale OOD benchmark that more explicitly evaluates feature extractors (*i.e.*, when zooming is controlled to provide no advantages).

#### 4.8.1 The creation of ImageNet-Hard

**Data collection** We take CLIP ViT-L/14 (*i.e.*, the highest-performing CLIP available) and run the zooming procedure to find “Unclassifiable images” in Sec. 4.1 on each of the following datasets: IN-ReaL, IN-A, IN-R, IN-S, and ON. That is, for each image  $x$ , we generate 324 zoomed versions of  $x$  and feed them into CLIP ViT-L/14. We add  $x$  into ImageNet-Hard only if none of the 324 versions are correctly classified.

**ImageNet-C** To find a subset of IN-C images for adding into ImageNet-Hard, we first re-generate ImageNet-C by adding the 19 types of corruption noise to IN without resizing the original IN images. That is, the original IN-C [22] contains exclusively pre-processed images already cropped to  $224 \times 224$ , which significantly makes the classification task unnecessarily more ill-posed (*e.g.*, by adding Gaussian noise to a crop where the main object is already removed).

Second, we run CLIP ViT-L/14 on all 19 types and manually select a subset of six diverse and lowest-accuracy corruption types of *Impulse Noise*, *Frost*, *Fog*, *Snow*, *Brightness*, and *Zoom Blur*. We repeat the data collection above to these 6 image sets.

**Groundtruth labels** After the above procedure, our dataset contains a total of 13,925 images collected from IN+ReaL, IN-A, IN-C, IN-R, IN-S, and ON (see the distribution in Appendix E). We manually inspect all images and remove 295 images that are obviously ill-posed (*e.g.* an entirely black image but labeled `great white shark` in IN-S), resulting in a final total of 13,630 ImageNet-Hard images. All images contain one original groundtruth label from their corresponding datasets except for IN and IN-C images, which has a set of IN+ReaL labels. An IN or IN-C image is considered correctly classified by a model if its top-1 predicted label is among the set of groundtruth labels.

**Release** ImageNet-Hard can be viewed and downloaded on [HuggingFace](#). Our code for evaluating state-of-the-art models on ImageNet-Hard is on [Github](#).

#### 4.8.2 Evaluating classifiers on ImageNet-Hard

To evaluate the performance of popular state-of-the-art classifiers on ImageNet-Hard, we follow the standard practice. We use the 1-crop evaluation to resize and center-crop a  $224 \times 224$  px region from each test image.

In addition to classifiers tested so far, we include CLIP-ViT-L/14@336px [44] and EfficientNet [66], both of which are state-of-the-art models that operate at higher image resolutions of  $336 \times 336$ , and  $800 \times 800$  respectively.

Table 6: Top-1 accuracy (%) on ImageNet-Hard. All models operate at  $224 \times 224$  except for the last two models.

Classifier	Accuracy	Classifier	Accuracy
ResNet-18	9.41	ViT-B/32	15.95
ResNet-50	12.56	CLIP-ViT-L/14@224px	1.86
VGG19	10.32	CLIP-ViT-L/14@336px	2.02
AlexNet	6.35	EfficientNet-L2@800px	34.23

**Results** Table 6 shows the top-1 accuracy of various classifiers on the ImageNet-Hard dataset. Our results suggest that ImageNet-Hard poses a significant challenge to state-of-the-art models. Among standard IN-trained classifiers, ViT-B/32 achieves the best top-1 accuracy (15.95%), followed by ResNet-50 (12.56%).

Among all 8 tested models, EfficientNet-L2 obtains the highest accuracy 34.23% (compared to 88.40% [66] on the original ImageNet). Overall, all models perform substantially worse on ImageNet-Hard than on other OOD datasets (see Tab. A2; 1-crop).

The performance of the two tested CLIP ViT-L/14 models (at two different resolutions) is noticeably lower than that of the other evaluated classifiers is hypothesized to be because ImageNet-Hard was specifically constructed based on images misclassified by CLIP ViT-L/14@224.

Our results suggest that ImageNet-Hard is a new challenging dataset and suitable for benchmarking the OOD robustness of state-of-the-art image classifiers.

## 5. Discussion and Conclusion

We conducted a novel, rigorous study on the effect of zooming over a set of six well-known classifiers and six image classification benchmarks. We are the first to show that previous state-of-the-art classifiers, as old as AlexNet [31], could potentially reach a surprisingly high accuracy (near 90%) if optimal zooming is provided. That finding raises the interesting question of whether the evolution of image classifiers over the last decade amounts to learning where to zoom and at which scale (as opposed to improving the feature extractors to more accurately describe a single object *a.k.a.* representation learning [2]).

We are also the first to document the spatial biases of existing benchmarks. Especially, IN-A and ON contain a large center bias and simply zooming to the center will de-clutter the scene and yield a high accuracy (24.69% for ViT-B/32 on IN-A; Tab. 4), which is competitive with state-of-the-art trained models (*e.g.* 24.1% of Robust ViT [10]) and much higher than state-of-the-art TTA techniques (*e.g.* 11.21% of MEMO [69]; Tab. 5). Our simple, but strong zoom-in baselines on IN-A and ON motivate future research into better-controlled benchmarks that more explicitly test models on a set of pre-defined properties. Our proposed TTA method

with zoom-in transforms (MEMO + RRC) is not only more accurate but also more interpretable and faster to run than the original MEMO.

Finally, we introduce ImageNet-Hard (Sec. 4.8), a new challenging dataset for IN-trained and other state-of-the-art classifiers.

## Acknowledgements

GN is supported by Auburn University PGRF Fellowship. AN was supported by NSF Grant No. 2145767, and donations from NaphCare Foundation, and Adobe Research.

## References

- [1] Centercrop — torchvision main documentation. <https://pytorch.org/vision/main/generated/torchvision.transforms.CenterCrop.html>. (Accessed on 03/07/2023). 6
- [2] Iclr 2023. <https://iclr.cc/>. (Accessed on 11/10/2022). 9
- [3] Randomresizedcrop — torchvision main documentation. <https://pytorch.org/vision/main/generated/torchvision.transforms.RandomResizedCrop.html>. (Accessed on 03/08/2023). 8
- [4] Michael A Alcorn, Qi Li, Zhitao Gong, Chengfei Wang, Long Mai, Wei-Shinn Ku, and Anh Nguyen. Strike (with) a pose: Neural networks are easily fooled by strange poses of familiar objects. In *Proceedings of the IEEE/CVF conference on computer vision and pattern recognition*, pages 4845–4854, 2019. 8
- [5] Murat Seckin Ayhan and Philipp Berens. Test-time data augmentation for estimation of heteroscedastic aleatoric uncertainty in deep neural networks. In *Medical Imaging with Deep Learning*, 2018. 2
- [6] Yuval Bahat and Gregory Shakhnarovich. Classification confidence estimation with test-time data-augmentation. *arXiv e-prints*, pages arXiv–2006, 2020. 2
- [7] Andrei Barbu, David Mayo, Julian Alverio, William Luo, Christopher Wang, Dan Gutfreund, Josh Tenenbaum, and Boris Katz. Objectnet: A large-scale bias-controlled dataset for pushing the limits of object recognition models. *Advances in neural information processing systems*, 32, 2019. 2, 3, 8
- [8] David Bau, Bolei Zhou, Aditya Khosla, Aude Oliva, and Antonio Torralba. Network dissection: Quantifying interpretability of deep visual representations. In *Proceedings of the IEEE conference on computer vision and pattern recognition*, pages 6541–6549, 2017. 1
- [9] Lucas Beyer, Olivier J Hénaff, Alexander Kolesnikov, Xiaohua Zhai, and Aaron van den Oord. Are we done with imagenet? *arXiv preprint arXiv:2006.07159*, 2020. 2, 3
- [10] Hila Chefer, Idan Schwartz, and Lior Wolf. Optimizing relevance maps of vision transformers improves robustness. In Alice H. Oh, Alekh Agarwal, Danielle Belgrave, and Kyunghyun Cho, editors, *Advances in Neural Information Processing Systems*, 2022. 9
- [11] Peijie Chen, Chirag Agarwal, and Anh Nguyen. The shape and simplicity biases of adversarially robust imagenet-trained cnns. *arXiv preprint arXiv:2006.09373*, 2020. 5
- [12] Sizhe Chen, Xiaolin Huang, Zhengbao He, and Chengjin Sun. Damagenet: A universal adversarial dataset. *arXiv preprint arXiv:1912.07160*, 2019. 8
- [13] Sewhan Chun, Jae Young Lee, and Junmo Kim. Cyclic test time augmentation with entropy weight method. In *Uncertainty in Artificial Intelligence*, pages 433–442. PMLR, 2022. 2
- [14] Alexey Dosovitskiy, Lucas Beyer, Alexander Kolesnikov, Dirk Weissenborn, Xiaohua Zhai, Thomas Unterthiner, Mostafa Dehghani, Matthias Minderer, Georg Heigold, Sylvain Gelly, et al. An image is worth 16x16 words: Transformers for image recognition at scale. In *International Conference on Learning Representations*, 2020. 1, 3, 20, 34
- [15] Jianlong Fu, Heliang Zheng, and Tao Mei. Look closer to see better: Recurrent attention convolutional neural network for fine-grained image recognition. In *Proceedings of the IEEE conference on computer vision and pattern recognition*, pages 4438–4446, 2017. 2
- [16] Robert Geirhos, Jörn-Henrik Jacobsen, Claudio Michaelis, Richard Zemel, Wieland Brendel, Matthias Bethge, and Felix A Wichmann. Shortcut learning in deep neural networks. *Nature Machine Intelligence*, 2(11):665–673, 2020. 26
- [17] Robert Geirhos, Patricia Rubisch, Claudio Michaelis, Matthias Bethge, Felix A. Wichmann, and Wieland Brendel. Imagenet-trained CNNs are biased towards texture; increasing shape bias improves accuracy and robustness. In *International Conference on Learning Representations*, 2019. 5
- [18] Gabriel Goh, Nick Cammarata, Chelsea Voss, Shan Carter, Michael Petrov, Ludwig Schubert, Alec Radford, and Chris Olah. Multimodal neurons in artificial neural networks. *Distill*, 6(3):e30, 2021. 1, 4
- [19] Agrim Gupta, Piotr Dollar, and Ross Girshick. Lvis: A dataset for large vocabulary instance segmentation. In *Proceedings of the IEEE/CVF conference on computer vision and pattern recognition*, pages 5356–5364, 2019. 27
- [20] Kaiming He, Xiangyu Zhang, Shaoqing Ren, and Jian Sun. Deep residual learning for image recognition. In *Proceedings of the IEEE conference on computer vision and pattern recognition*, pages 770–778, 2016. 1, 2, 3, 7, 8, 20
- [21] Dan Hendrycks, Steven Basart, Norman Mu, Saurav Kadavath, Frank Wang, Evan Dorundo, Rahul Desai, Tyler Zhu, Samyak Parajuli, Mike Guo, et al. The many faces of robustness: A critical analysis of out-of-distribution generalization. In *Proceedings of the IEEE/CVF International Conference on Computer Vision*, pages 8340–8349, 2021. 3, 7, 8, 20, 29
- [22] Dan Hendrycks and Thomas Dietterich. Benchmarking neural network robustness to common corruptions and perturbations. *arXiv preprint arXiv:1903.12261*, 2019. 8, 9
- [23] Dan Hendrycks, Norman Mu, Ekin D Cubuk, Barret Zoph, Justin Gilmer, and Balaji Lakshminarayanan. Augmix: A simple data processing method to improve robustness and uncertainty. *arXiv preprint arXiv:1912.02781*, 2019. 7, 46



- [24] Dan Hendrycks, Kevin Zhao, Steven Basart, Jacob Steinhardt, and Dawn Song. Natural adversarial examples. In *Proceedings of the IEEE/CVF Conference on Computer Vision and Pattern Recognition*, pages 15262–15271, 2021. [2](#), [3](#), [8](#)
- [25] Andrew Howard, Mark Sandler, Grace Chu, Liang-Chieh Chen, Bo Chen, Mingxing Tan, Weijun Wang, Yukun Zhu, Ruoming Pang, Vijay Vasudevan, et al. Searching for mobilenetv3. In *Proceedings of the IEEE/CVF international conference on computer vision*, pages 1314–1324, 2019. [20](#)
- [26] Gao Huang, Zhuang Liu, Laurens Van Der Maaten, and Kilian Q Weinberger. Densely connected convolutional networks. In *Proceedings of the IEEE conference on computer vision and pattern recognition*, pages 4700–4708, 2017. [20](#)
- [27] Max Jaderberg, Karen Simonyan, Andrew Zisserman, et al. Spatial transformer networks. *Advances in neural information processing systems*, 28, 2015. [2](#)
- [28] Ildoo Kim, Younghoon Kim, and Sungwoong Kim. Learning loss for test-time augmentation. *Advances in Neural Information Processing Systems*, 33:4163–4174, 2020. [2](#)
- [29] Jon Kleinberg and Eva Tardos. *Algorithm Design*. Addison-Wesley Longman Publishing Co., Inc., USA, 2005. [4](#)
- [30] Fanjie Kong and Ricardo Henao. Efficient classification of very large images with tiny objects. In *Proceedings of the IEEE/CVF Conference on Computer Vision and Pattern Recognition*, pages 2384–2394, 2022. [2](#)
- [31] Alex Krizhevsky, Ilya Sutskever, and Geoffrey E Hinton. Imagenet classification with deep convolutional neural networks. *Advances in neural information processing systems*, 25, 2012. [1](#), [2](#), [3](#), [6](#), [7](#), [8](#), [9](#), [20](#)
- [32] Brandon Leung, Chih-Hui Ho, Amir Persekian, David Orozco, Yen Chang, Erik Sandstrom, Bo Liu, and Nuno Vasconcelos. Owl500: Overcoming dataset collection bias in the wild. *arXiv preprint arXiv:2108.10992*, 2021. [2](#)
- [33] Boyi Li, Felix Wu, Ser-Nam Lim, Serge Belongie, and Kilian Q Weinberger. On feature normalization and data augmentation. In *Proceedings of the IEEE/CVF Conference on Computer Vision and Pattern Recognition*, pages 12383–12392, 2021. [8](#), [20](#), [29](#)
- [34] Junnan Li, Caiming Xiong, and Steven CH Hoi. Learning from noisy data with robust representation learning. In *Proceedings of the IEEE/CVF International Conference on Computer Vision*, pages 9485–9494, 2021. [29](#)
- [35] Xiao Li, Jianmin Li, Ting Dai, Jie Shi, Jun Zhu, and Xiaolin Hu. Rethinking natural adversarial examples for classification models. *arXiv preprint arXiv:2102.11731*, 2021. [2](#)
- [36] Zhuang Liu, Hanzi Mao, Chao-Yuan Wu, Christoph Feichtenhofer, Trevor Darrell, and Saining Xie. A convnet for the 2020s. In *Proceedings of the IEEE/CVF Conference on Computer Vision and Pattern Recognition*, pages 11976–11986, 2022. [3](#), [20](#)
- [37] Alexandra Sasha Luccioni and David Rolnick. Bugs in the data: How imagenet misrepresents biodiversity. *arXiv preprint arXiv:2208.11695*, 2022. [2](#)
- [38] Alexander Lyzhov, Yuliya Molchanova, Arsenii Ashukha, Dmitry Molchanov, and Dmitry Vetrov. Greedy policy search: A simple baseline for learnable test-time augmentation. In *Conference on Uncertainty in Artificial Intelligence*, pages 1308–1317. PMLR, 2020. [2](#), [7](#)
- [39] Ningning Ma, Xiangyu Zhang, Hai-Tao Zheng, and Jian Sun. Shufflenet v2: Practical guidelines for efficient cnn architecture design. In *Proceedings of the European conference on computer vision (ECCV)*, pages 116–131, 2018. [20](#)
- [40] Sébastien Marcel and Yann Rodriguez. Torchvision the machine-vision package of torch. In *Proceedings of the 18th ACM international conference on Multimedia*, pages 1485–1488, 2010. [14](#)
- [41] Matthias Minderer, Alexey Gritsenko, Austin Stone, Maxim Neumann, Dirk Weissenborn, Alexey Dosovitskiy, Aravindh Mahendran, Anurag Arnab, Mostafa Dehghani, Zhuoran Shen, et al. Simple open-vocabulary object detection with vision transformers. *arXiv preprint arXiv:2205.06230*, 2022. [27](#), [28](#)
- [42] Anh Nguyen, Jason Yosinski, and Jeff Clune. Multifaceted feature visualization: Uncovering the different types of features learned by each neuron in deep neural networks. *arXiv preprint arXiv:1602.03616*, 2016. [1](#)
- [43] Tianyu Pang, Kun Xu, and Jun Zhu. Mixup inference: Better exploiting mixup to defend adversarial attacks. *arXiv preprint arXiv:1909.11515*, 2019. [2](#)
- [44] Alec Radford, Jong Wook Kim, Chris Hallacy, Aditya Ramesh, Gabriel Goh, Sandhini Agarwal, Girish Sastry, Amanda Askell, Pamela Mishkin, Jack Clark, et al. Learning transferable visual models from natural language supervision. In *International conference on machine learning*, pages 8748–8763. PMLR, 2021. [2](#), [3](#), [4](#), [9](#), [34](#)
- [45] Adria Recasens, Petr Kellnhofer, Simon Stent, Wojciech Matysik, and Antonio Torralba. Learning to zoom: a saliency-based sampling layer for neural networks. In *Proceedings of the European Conference on Computer Vision (ECCV)*, pages 51–66, 2018. [2](#)
- [46] Joshua Robinson, Li Sun, Ke Yu, Kayhan Batmanghelich, Stefanie Jegelka, and Suvrit Sra. Can contrastive learning avoid shortcut solutions? *Advances in neural information processing systems*, 34:4974–4986, 2021. [26](#)
- [47] Ramprasaath Rs, Michael Cogswell, Abhishek Das, Ramakrishna Vedantam, Devi Parikh, and Dhruv Batra. Grad-cam: Visual explanations from deep networks via gradient-based localization. *International Journal of Computer Vision*, 128, 02 2020. [1](#)
- [48] Olga Russakovsky, Jia Deng, Hao Su, Jonathan Krause, Sanjeev Satheesh, Sean Ma, Zhiheng Huang, Andrej Karpathy, Aditya Khosla, Michael Bernstein, et al. Imagenet large scale visual recognition challenge. *International Journal of Computer Vision*, 115(3):211–252, 2015. [1](#), [3](#), [26](#)
- [49] Mark Sandler, Andrew Howard, Menglong Zhu, Andrey Zhmoginov, and Liang-Chieh Chen. Mobilenetv2: Inverted residuals and linear bottlenecks. In *Proceedings of the IEEE conference on computer vision and pattern recognition*, pages 4510–4520, 2018. [20](#)
- [50] Ikuro Sato, Hiroki Nishimura, and Kensuke Yokoi. Apac: Augmented pattern classification with neural networks. *arXiv preprint arXiv:1505.03229*, 2015. [2](#), [7](#)

- [51] Divya Shanmugam, Davis Blalock, Guha Balakrishnan, and John Guttag. Better aggregation in test-time augmentation. In *Proceedings of the IEEE/CVF International Conference on Computer Vision*, pages 1214–1223, 2021. 2
- [52] Karen Simonyan and Andrew Zisserman. Very deep convolutional networks for large-scale image recognition. *arXiv preprint arXiv:1409.1556*, 2014. 2, 3, 7, 20
- [53] Petr Slavík. A tight analysis of the greedy algorithm for set cover. In *Proceedings of the Twenty-Eighth Annual ACM Symposium on Theory of Computing*, STOC '96, page 435–441, New York, NY, USA, 1996. Association for Computing Machinery. 4
- [54] Lewis Smith and Yarin Gal. Understanding measures of uncertainty for adversarial example detection. *arXiv preprint arXiv:1803.08533*, 2018. 2
- [55] Andreas Steiner, Alexander Kolesnikov, Xiaohua Zhai, Ross Wightman, Jakob Uszkoreit, and Lucas Beyer. How to train your vit? data, augmentation, and regularization in vision transformers. *arXiv preprint arXiv:2106.10270*, 2021. 29
- [56] Yu Sun, Xiaolong Wang, Zhuang Liu, John Miller, Alexei Efros, and Moritz Hardt. Test-time training with self-supervision for generalization under distribution shifts. In *International conference on machine learning*, pages 9229–9248. PMLR, 2020. 2
- [57] Christian Szegedy, Wei Liu, Yangqing Jia, Pierre Sermanet, Scott Reed, Dragomir Anguelov, Dumitru Erhan, Vincent Vanhoucke, and Andrew Rabinovich. Going deeper with convolutions. In *Proceedings of the IEEE conference on computer vision and pattern recognition*, pages 1–9, 2015. 2
- [58] Mohammad Reza Taesiri, Giang Nguyen, and Anh Nguyen. Visual correspondence-based explanations improve ai robustness and human-ai team accuracy. In *Advances in Neural Information Processing Systems*. 2
- [59] Mingxing Tan and Quoc Le. Efficientnet: Rethinking model scaling for convolutional neural networks. In *International conference on machine learning*, pages 6105–6114. PMLR, 2019. 20
- [60] Dimitris Tsipras, Shibani Santurkar, Logan Engstrom, Andrew Ilyas, and Aleksander Madry. From imagenet to image classification: Contextualizing progress on benchmarks. In *International Conference on Machine Learning*, pages 9625–9635. PMLR, 2020. 2
- [61] Burak Uzkent and Stefano Ermon. Learning when and where to zoom with deep reinforcement learning. In *Proceedings of the IEEE/CVF conference on computer vision and pattern recognition*, pages 12345–12354, 2020. 2
- [62] Dequan Wang, Evan Shelhamer, Shaoteng Liu, Bruno Olshausen, and Trevor Darrell. Tent: Fully test-time adaptation by entropy minimization. In *International Conference on Learning Representations*, 2020. 2
- [63] Haohan Wang, Songwei Ge, Zachary Lipton, and Eric P Xing. Learning robust global representations by penalizing local predictive power. *Advances in Neural Information Processing Systems*, 32, 2019. 2, 3, 8
- [64] Ross Wightman, Hugo Touvron, and Hervé Jégou. Resnet strikes back: An improved training procedure in timm. *arXiv preprint arXiv:2110.00476*, 2021. 29
- [65] Kai Yuanqing Xiao, Logan Engstrom, Andrew Ilyas, and Aleksander Madry. Noise or signal: The role of image backgrounds in object recognition. In *International Conference on Learning Representations*, 2020. 26
- [66] Qizhe Xie, Minh-Thang Luong, Eduard Hovy, and Quoc V Le. Self-training with noisy student improves imagenet classification. In *Proceedings of the IEEE/CVF conference on computer vision and pattern recognition*, pages 10687–10698, 2020. 9
- [67] Saining Xie, Ross Girshick, Piotr Dollár, Zhuowen Tu, and Kaiming He. Aggregated residual transformations for deep neural networks. In *Proceedings of the IEEE conference on computer vision and pattern recognition*, pages 1492–1500, 2017. 20
- [68] Sergey Zagoruyko and Nikos Komodakis. Wide residual networks. *arXiv preprint arXiv:1605.07146*, 2016. 20
- [69] Marvin Zhang, Sergey Levine, and Chelsea Finn. Memo: Test time robustness via adaptation and augmentation. *arXiv preprint arXiv:2110.09506*, 2021. 2, 7, 8, 9, 20
- [70] Marvin Zhang, Henrik Marklund, Nikita Dhawan, Abhishek Gupta, Sergey Levine, and Chelsea Finn. Adaptive risk minimization: Learning to adapt to domain shift. *Advances in Neural Information Processing Systems*, 34:23664–23678, 2021. 2
- [71] Yiwu Zhong, Jianwei Yang, Pengchuan Zhang, Chunyuan Li, Noel Codella, Liunian Harold Li, Luowei Zhou, Xiyang Dai, Lu Yuan, Yin Li, et al. Regionclip: Region-based language-image pretraining. In *Proceedings of the IEEE/CVF Conference on Computer Vision and Pattern Recognition*, pages 16793–16803, 2022. 7
- [72] Zhuotun Zhu, Lingxi Xie, and Alan L Yuille. Object recognition with and without objects. *arXiv preprint arXiv:1611.06596*, 2016. 26

---

## Appendix for: **Zoom $\oplus$ is what you need: An empirical study of the power of zoom and spatial biases in image classification**

---

### A. Implementation details

In this section, we provide a detailed description of our experimental setup, including the Python code for our zoom transform, the classifiers we employed, and the setup we used for zero-shot classification.

#### A.1. Sample Python code for zoom-based transform

```
from PIL import Image
import torchvision.transforms.functional as fv
import torchvision.transforms as transforms
from functools import partial

def crop_at(size, slice_x, slice_y):
    def slice_crop(image, size, slice_x, slice_y):
        width, height = image.size
        tile_size_x = width // 3
        tile_size_y = height // 3
        anchor_x = (slice_y * tile_size_x) + (tile_size_x // 2)
        anchor_y = (slice_x * tile_size_y) + (tile_size_y // 2)
        return fv.crop(
            image,
            anchor_y - (size // 2),
            anchor_x - (size // 2),
            size,
            size,
        )
    return partial(slice_crop, size=size, slice_x=slice_x, slice_y=slice_y)

zoom_scale = 255
zoom_transform = transforms.Compose(
    [
        transforms.Resize(
            zoom_scale,
            interpolation=transforms.InterpolationMode.BICUBIC,
            max_size=None,
            antialias=None,
        ),
        crop_at(224, i, j),
    ]
)
```

Code. A1: Sample python code.



## A.2. Zoom Scales used

In our experiments, we tried the following zoom scales:

10, 16, 32, 48, 64, 96, 122, 128, 192, 224, 235, 240, 256, 288, 320, 348, 384, 448, 460, 512, 573, 576, 640, 664, 672, 680, 686, 690, 700, 720, 768, 798, 832, 896, 911, 1024

## A.3. Model selection

We use the official OpenAI library<sup>2</sup> for CLIP. All other models and weights are retrieved from the `torchvision` [40] library.

## A.4. Zero-shot classification using CLIP

For CLIP, we follow the standard zero-shot classification. This involves creating a text template for each class in the dataset, which contains a generic description of an image featuring an object from that class. Then, we use CLIP’s text encoder to obtain embeddings for these templates and then average them to obtain a final vector that represents the class. To classify an image, we calculate the cosine similarity between its embedding and the text vectors for each class and then select the class with the highest value.

## A.5. Zoom-based transform

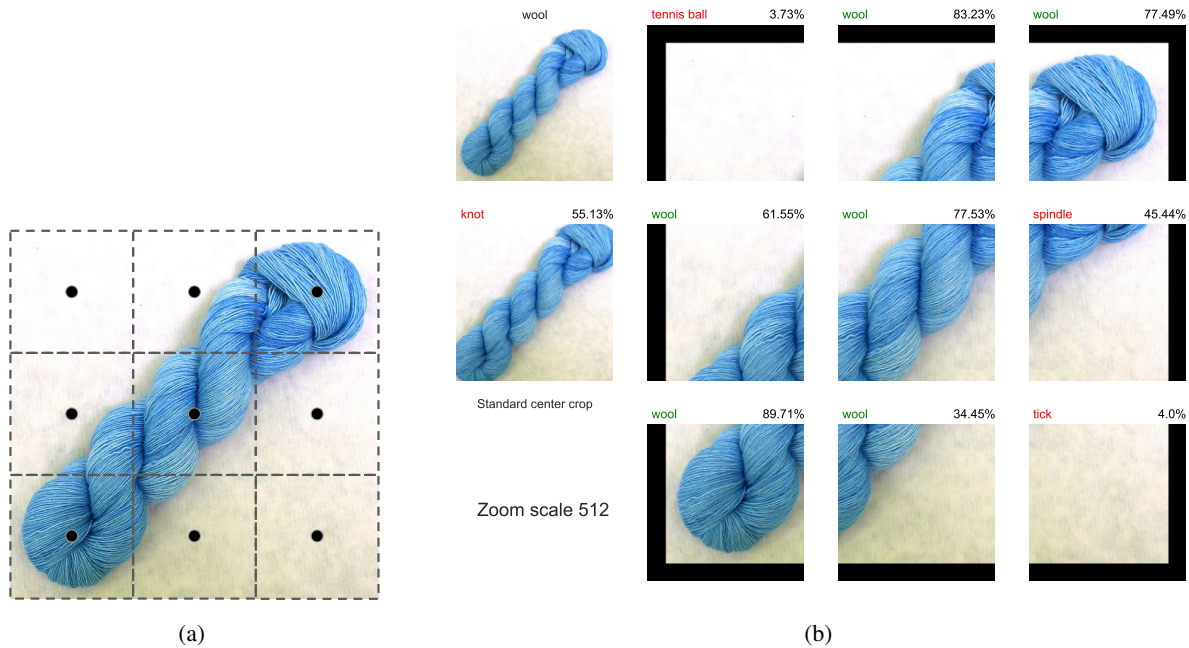


Figure A2: (a) Making a 3-by-3 uniform grid out of the image. We pick the center point in each region as the anchor. (b) Sample image showing how our zoom transform is applied to an image.

<sup>2</sup><https://github.com/openai/CLIP>

## B. Additional Results

In this section, we provide additional results for our experiments.

### B.1. Zooming out is needed for a small portion of the datasets

In our approach, we leverage the power of both zoom-in and zoom-out transforms, and Tab. 1 results indicate that this combined zooming approach can be effective in classifying images from diverse datasets. Zooming in enhances texture patterns while zooming out provides a better perspective of the object’s shape. The question we aim to answer is which dataset and model pairs require which type of zoom, and whether zooming is always necessary. Additionally, we investigate which types of networks are less reliant on explicit zooming, as they implicitly focus on the main object in the image.

**Experiment** We separate zoom transforms into three groups and report the maximum possible accuracy as defined in Sec. 3. We use transforms in the minimum set covers (as shown in Tab. 2) for each dataset and classifier pair. We then report the number of images that can only be classified using transforms in each group separately.

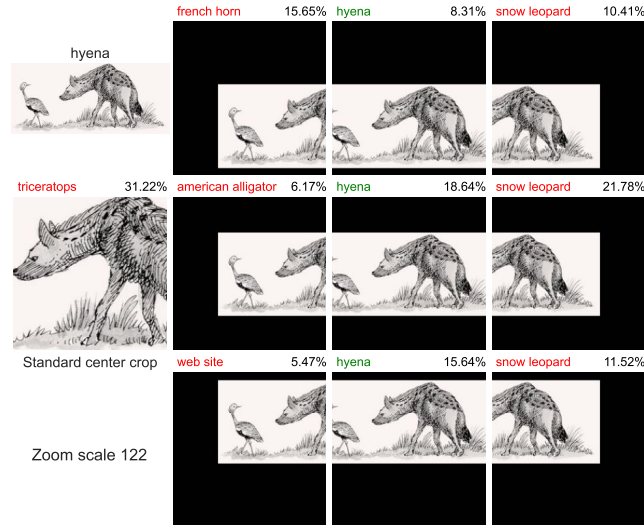


Figure A3: A sample image from the ImageNet-Sketch dataset that can only be solved by zooming out. For this image, with the standard ImageNet transform, the entire body of the animal is not visible. Instead, zooming out of the image helps you see the whole body of the animal. More samples can be found in Appendix D.3.

**Results** In general, we find that zooming in is more effective than zooming out. Zooming in provides two benefits: (1) it helps the model to focus on the key region where the target object is located, and (2) the model can extract features from the target object at a higher resolution. Across all methods and datasets, we can see a certain percentage of images are only classifiable using transforms of the *zoom-out* group. In particular, for ImageNet-R and ImageNet-Sketch, between 1.2% – 3% (Table A1) of the entire dataset can only be solved using a transform in the *zoom-out* group. This is especially true for drawings, where the texture may lack distinguishable features, and zooming out allows us to better perceive the shape.

Table A1: Breakdown of maximum possible accuracy by different zoom groups. In each dataset, certain images necessitate a specific zoom group for correct classification regardless of the model being used. However, CLIP performs well overall without depending heavily on a particular zoom level. On average, the percentage of datasets that can only be solved with a specific zoom group is very small for this model.

Dataset	Model	zoom-in Solve	zoom-out Solves	zoom-224 Solves	Only zoom-in Solves	Only zoom-out Solves	Only zoom-224 Solves
ImageNet	ResNet-18	94.57	79.49	81.16	10.59	0.43	0.08
	ResNet-50	96.30	85.84	86.39	7.59	0.40	0.04
	ViT-B/32	96.83	86.18	85.12	7.59	0.30	0.02
	VGG-16	94.60	82.11	83.08	8.92	0.58	0.07
	AlexNet	89.17	62.92	67.98	18.01	0.65	0.18
	CLIP-ViT-L/14	95.82	90.80	87.04	4.81	0.83	0.05
ImageNet Real	ResNet-18	97.37	86.10	87.62	7.38	0.27	0.07
	ResNet-50	98.22	91.07	91.87	4.65	0.25	0.04
	ViT-B/32	98.50	90.79	88.06	4.92	0.18	0.03
	VGG-16	97.38	88.43	89.40	6.02	0.38	0.07
	AlexNet	93.15	69.58	74.85	15.47	0.45	0.19
	CLIP-ViT-L/14	98.05	94.44	91.69	3.20	0.55	0.04
ImageNet+Real	ResNet-18	97.16	85.51	86.77	7.72	0.28	0.05
	ResNet-50	98.25	91.10	91.77	4.60	0.24	0.03
	ViT-B/32	98.70	91.00	90.95	4.92	0.14	0.02
	VGG-16	97.12	87.88	89.09	6.25	0.42	0.06
	AlexNet	92.79	68.65	73.93	16.25	0.47	0.16
	CLIP-ViT-L/14	98.24	95.09	92.41	2.75	0.47	0.04
ImageNet-A	ResNet-18	63.66	47.95	45.37	13.97	2.75	0.21
	ResNet-50	65.28	52.36	48.59	12.05	3.13	0.22
	ViT-B/32	73.07	56.34	54.84	14.20	2.04	0.27
	VGG-16	56.67	44.95	39.35	11.80	3.85	0.24
	AlexNet	52.69	32.86	31.95	17.15	2.34	0.30
	CLIP-ViT-L/14	98.35	96.71	93.57	1.70	0.69	0.04
ImageNet-R	ResNet-18	57.07	12.19	10.07	40.67	0.92	0.19
	ResNet-50	64.52	12.95	10.36	48.72	1.00	0.23
	ViT-B/32	76.71	18.57	21.92	51.75	0.85	0.15
	VGG-16	56.59	13.15	13.27	38.24	0.93	0.29
	AlexNet	39.91	10.39	9.11	26.27	1.08	0.36
	CLIP-ViT-L/14	97.99	81.32	77.03	12.01	0.44	0.05
ImageNet-Sketch	ResNet-18	41.14	27.06	27.41	11.83	1.77	0.36
	ResNet-50	44.72	32.80	31.45	10.99	2.23	0.24
	ViT-B/32	53.45	37.43	37.38	13.11	1.83	0.36
	VGG-16	36.20	27.20	24.59	9.47	2.97	0.28
	AlexNet	27.71	13.84	15.11	11.26	1.22	0.33
	CLIP-ViT-L/14	86.20	80.67	73.94	6.64	2.38	0.12
ObjectNet	ResNet-18	68.98	38.52	37.23	25.76	1.93	0.25
	ResNet-50	74.16	51.56	47.79	19.68	2.16	0.30
	ViT-B/32	77.66	44.49	42.65	27.43	1.34	0.20
	VGG-16	69.19	41.72	39.49	23.34	2.27	0.31
	AlexNet	56.76	23.45	22.59	28.85	2.27	0.33
	CLIP-ViT-L/14	91.28	82.22	77.60	8.37	1.38	0.15
Average	ResNet-18	74.28	53.83	53.66	16.85	1.19	0.17
	ResNet-50	77.35	59.67	58.32	15.47	1.34	0.16
	ViT-B/32	82.13	60.69	60.13	17.70	0.95	0.15
	VGG-16	72.54	55.06	54.04	14.86	1.63	0.19
	AlexNet	64.60	40.24	42.22	19.04	1.21	0.26
	CLIP-ViT-L/14	95.13	88.75	84.75	5.64	0.95	0.07



## B.2. Performance of various aggregating methods

Table A2: Performance of various aggregating methods (%) – The bold numbers show maximum accuracy per model/dataset. CLIP strongly and consistently favors 10-crop over other settings.

Classifier	Dataset	(a)	(b) <i>zoom-in</i>		(c) <i>zoom-out</i>		(d) <i>zoom-224</i>		(e) 5-crop		(f) 10-crop	
		1-crop	Max	Mean	Max	Mean	Max	Mean	Max	Mean	Max	Mean
ResNet-18	IN	69.45	68.45 (-1.00)	71.45 (+2.00)	60.33	56.79	67.85	68.70	70.61	71.32	70.83	<b>71.85</b>
	ReaL	76.94	76.33 (-0.61)	<b>79.94</b> (+3.00)	67.64	63.92	75.73	76.74	78.26	79.01	78.42	79.46
	IN-A	1.37	<b>11.68</b> (+10.31)	5.48 (+4.11)	2.44	2.19	3.41	2.69	3.16	2.13	3.28	1.87
	IN-R	32.14	30.60 (-1.54)	28.95 (-3.19)	29.08	27.28	32.29	32.54	33.99	33.38	<b>34.59</b>	33.83
	IN-S	19.41	14.86 (-4.55)	14.34 (-5.07)	14.48	11.49	17.80	17.83	20.83	20.70	<b>21.39</b>	21.06
	ON	27.59	<b>28.21</b> (+0.62)	25.92 (-1.67)	16.11	14.10	22.82	22.86	24.77	20.91	25.47	21.03
ResNet-50	IN	75.75	73.24 (-2.51)	77.30 (+1.55)	69.06	66.42	74.45	75.39	76.67	77.13	76.89	<b>77.43</b>
	ReaL	82.63	80.36 (-2.27)	<b>84.68</b> (+2.05)	76.35	73.85	81.96	82.85	83.67	84.06	83.82	84.31
	IN-A	0.21	<b>16.11</b> (+15.9)	6.23 (+6.02)	2.79	2.19	3.04	2.11	2.28	0.95	2.43	1.00
	IN-R	35.39	33.58 (-1.81)	32.73 (-2.66)	35.85	33.22	36.64	36.44	37.47	36.50	<b>38.23</b>	36.86
	IN-S	22.91	16.89 (-6.02)	17.80 (-5.11)	19.51	17.12	21.60	21.66	24.71	24.51	<b>24.94</b>	24.74
	ON	<b>36.18</b>	34.56 (-1.62)	34.22 (-1.96)	27.10	25.32	31.78	31.98	33.34	29.58	33.93	29.86
ViT-B/32	IN	75.75	74.35 (-1.40)	<b>79.31</b> (+3.56)	71.48	69.47	72.66	73.67	77.33	77.73	77.30	77.87
	ReaL	81.89	80.22 (-1.67)	<b>85.97</b> (+4.08)	77.95	76.28	79.25	80.31	83.24	83.80	83.17	83.87
	IN-A	9.64	<b>24.69</b> (+15.05)	14.29 (+4.65)	7.79	5.48	8.12	7.39	12.19	9.88	12.32	9.67
	IN-R	41.29	39.90 (-1.39)	40.06 (-1.23)	39.05	36.21	39.52	39.28	43.90	43.17	<b>44.31</b>	43.28
	IN-S	26.83	19.74 (-7.09)	20.89 (-5.94)	22.37	19.25	25.06	25.21	28.72	28.66	<b>28.94</b>	28.76
	ON	30.89	32.88 (+1.99)	<b>33.92</b> (+3.03)	22.56	19.51	22.75	22.72	26.96	24.98	27.14	24.97
VGG-16	IN	71.37	69.60 (-1.77)	72.46 (+1.09)	64.75	59.95	69.51	70.48	72.31	73.09	72.67	<b>73.53</b>
	ReaL	78.90	77.23 (-1.67)	80.59 (+1.69)	72.55	67.68	77.48	78.58	79.80	80.42	80.13	<b>80.80</b>
	IN-A	2.69	<b>11.55</b> (+8.86)	6.24 (+3.55)	3.33	2.77	4.69	3.87	4.87	3.19	5.09	3.19
	IN-R	26.98	26.18 (-0.80)	24.74 (-2.24)	28.01	25.62	27.76	27.78	28.75	27.95	<b>29.23</b>	28.35
	IN-S	16.78	13.30 (-3.48)	13.05 (-3.73)	15.18	13.37	15.82	15.97	17.80	17.63	<b>18.28</b>	17.92
	ON	<b>28.32</b>	26.96 (-1.36)	26.15 (-2.17)	19.88	16.42	23.47	23.60	26.21	21.65	26.52	21.80
AlexNet	IN	56.16	54.74 (-1.42)	56.98 (+0.82)	40.78	27.09	51.80	51.50	57.86	58.60	58.26	<b>59.11</b>
	ReaL	62.67	61.46 (-1.21)	64.35 (+1.68)	45.84	30.58	58.25	58.16	64.53	65.39	64.98	<b>65.94</b>
	IN-A	1.75	<b>4.65</b> (+2.90)	3.27 (+1.52)	1.56	1.23	2.31	1.97	2.53	2.04	2.64	2.03
	IN-R	21.10	20.65 (-0.45)	17.97 (-3.13)	15.72	11.25	19.91	19.55	22.79	21.86	<b>23.26</b>	22.16
	IN-S	10.05	7.94 (-2.11)	6.54 (-3.51)	5.82	2.72	8.29	7.39	10.84	10.65	<b>11.20</b>	10.80
	ON	14.23	<b>14.91</b> (+0.68)	11.80 (-2.43)	6.11	3.75	9.65	9.01	12.63	9.57	12.84	9.58
CLIP-ViT-L/14	IN	75.03	70.01 (-5.02)	74.45 (-0.58)	72.01	72.21	74.45	76.04	76.77	76.91	76.72	<b>77.00</b>
	ReaL	80.68	76.37 (-4.31)	81.31 (+0.63)	78.28	78.93	81.45	82.05	82.26	<b>82.55</b>	82.26	<b>82.55</b>
	IN-A	71.28	76.57 (+5.29)	68.16 (-3.12)	60.71	49.51	71.69	70.04	77.80	76.61	<b>78.25</b>	76.83
	IN-R	87.74	84.12 (-3.62)	83.54 (-4.20)	86.84	86.29	88.12	88.24	89.64	89.66	<b>90.01</b>	89.94
	IN-S	58.23	51.88 (-6.35)	56.06 (-2.17)	57.14	57.43	59.00	59.90	61.28	61.61	61.59	<b>62.07</b>
	ON	66.32	60.20 (-6.12)	58.10 (-8.22)	56.57	58.11	62.44	62.65	66.70	64.88	<b>66.87</b>	64.97

### B.3. Anchor-based analysis of Center bias in ImageNet and OOD datasets

91.58	93.49	91.74	19.35	22.21	19.21	54.42	57.41	54.66	34.47	37.05	34.62	34.15	35.87	34.34
93.33	95.21	93.46	23.87	39.09	23.41	56.70	60.14	56.89	36.29	39.34	36.43	53.14	62.66	53.39
91.87	93.71	92.03	20.20	23.21	19.88	53.78	56.52	53.84	33.71	36.04	33.77	35.11	36.66	35.06
(a) ImageNet-ReaL			(b) ImageNet-A			(c) ImageNet-R			(d) ImageNet-Sketch			(e) ObjectNet		

Figure A4: ResNet-18

94.53	95.82	94.82	21.17	26.77	21.59	57.55	60.28	57.59	38.88	41.08	39.01	46.81	47.96	46.85
95.58	96.77	95.91	27.57	46.49	26.57	59.49	62.52	59.62	40.57	42.92	40.71	62.25	69.30	62.53
94.65	95.92	94.94	22.52	27.61	22.31	57.09	59.60	57.19	38.29	40.38	38.37	48.42	49.84	48.55
(a) ImageNet-ReaL			(b) ImageNet-A			(c) ImageNet-R			(d) ImageNet-Sketch			(e) ObjectNet		

Figure A5: ResNet-50

94.45	95.55	94.14	32.72	38.48	33.21	63.91	66.87	64.06	46.29	48.88	46.29	40.16	41.54	40.40
95.61	96.86	95.41	40.28	59.92	39.49	65.79	69.45	65.96	47.86	50.84	47.80	59.80	69.52	59.93
94.70	95.80	94.26	34.51	40.13	33.13	62.81	65.31	62.82	44.83	46.91	44.73	41.95	43.88	42.02
(a) ImageNet-ReaL			(b) ImageNet-A			(c) ImageNet-R			(d) ImageNet-Sketch			(e) ObjectNet		

Figure A6: ViT-B/32

92.77	94.20	92.72	21.83	26.35	21.95	50.04	51.98	49.86	32.43	34.25	32.13	37.42	38.70	37.42
94.13	95.52	94.02	26.97	39.36	26.19	51.76	54.28	51.71	33.92	35.91	33.63	54.41	62.45	54.66
92.83	94.41	93.04	22.03	27.37	21.99	49.40	51.35	49.31	31.60	33.30	31.35	37.74	39.07	37.86
(a) ImageNet-ReaL			(b) ImageNet-A			(c) ImageNet-R			(d) ImageNet-Sketch			(e) ObjectNet		

Figure A7: VGG16

81.72	85.25	81.62
84.88	88.78	84.70
81.91	85.35	81.76

(a) ImageNet-Real

15.93	17.24	15.00
19.01	25.51	17.51
16.79	18.89	16.20

(b) ImageNet-A

40.39	43.67	40.20
43.05	47.22	42.97
39.67	42.88	39.58

(c) ImageNet-R

20.64	23.07	20.64
22.26	25.14	22.20
19.73	21.88	19.70

(d) ImageNet-Sketch

21.42	22.49	21.42
38.20	48.16	38.35
21.15	22.42	21.08

(e) ObjectNet

Figure A8: AlexNet

92.42	93.67	92.76
93.64	94.44	93.70
92.59	93.86	92.62

(a) ImageNet-Real

77.31	85.04	77.53
85.41	92.31	84.65
77.60	84.49	77.29

(b) ImageNet-A

94.57	95.92	94.64
95.87	97.07	95.80
94.15	95.42	94.26

(c) ImageNet-R

74.57	77.28	74.65
77.08	79.43	77.19
73.61	76.24	73.62

(d) ImageNet-Sketch

66.81	70.03	67.88
82.06	86.97	81.87
68.32	71.38	68.46

(e) ObjectNet

Figure A9: CLIP-ViT-L/14

#### B.4. Distribution of the minimum set cover per classifier and dataset

In this section, we provide details on the distribution of minimum set cover size.

Table A3: Distribution of the minimum set cover per classifier and dataset. (ZI: *zoom-in*, ZO: *zoom-out*, ZL: *zoom-224*)

	ReaL				IN-A				IN-R				IN-Sketch				ON			
	ZI	ZO	ZL	Total	ZI	ZO	ZL	Total	ZI	ZO	ZL	Total	ZI	ZO	ZL	Total	ZI	ZO	ZL	Total
ResNet-18	160	33	8	201	174	31	6	211	204	65	9	278	209	51	9	269	191	54	9	254
ResNet-50	136	33	9	178	165	42	7	214	200	62	9	271	216	56	9	281	187	63	9	259
ViT-B/32	134	30	4	168	167	19	7	193	196	52	9	257	218	46	9	273	206	58	9	273
VGG-16	158	34	9	201	181	33	8	222	214	66	9	289	210	54	9	273	198	52	9	259
AlexNet	191	40	8	239	170	33	9	212	212	51	9	272	217	49	9	275	201	58	9	268
CLIP-ViT-L/14	141	48	8	197	75	14	4	93	76	33	5	114	142	61	9	212	205	66	9	280

#### B.5. Runtime analysis of MEMO

Table A4: Average runtime per query image (in seconds). Using RandomResizedCrop in MEMO speed ups the runtime by an average factor of  $1.6\times$ .

Runtime (in seconds)	IN	IN-A	IN-R	IN-S	ON
MEMO + AugMix [69]					
ResNet-50 [20]	1.24	1.12	1.12	1.32	1.51
DeepAug+AugMix [21]	1.19	1.07	1.12	1.23	1.55
MoEx+CutMix [33]	1.15	1.16	1.11	1.31	1.53
MEMO + RRC ( <b>Ours</b> )					
ResNet-50 [20]	0.64	0.60	0.65	0.88	1.19
DeepAug+AugMix [21]	0.62	0.62	0.64	0.87	1.18
MoEx+CutMix [33]	0.65	0.62	0.66	0.88	1.19

#### B.6. 1-crop accuracy with different zoom scales

In this section, we demonstrate the performance of various models when zooming in or out of an image. In other words, we utilize the standard 1-crop ImageNet transform while altering the initial scale of the image.

In this section, we are conducting experiments using the following models: AlexNet [31], ConvNext (Base, Large, Small, Tiny) [36], DenseNet-161 [26], EfficientNet-B7 [59], MobileNet (V2, V3 Large) [25, 49], ResNet (50, 101) [20], ResNeXt-50 (32x4d) [67], ShuffleNet V2 x1.0 [39], VGG-19 [52], Vision Transformer (ViT-B/16, ViT-B/32, ViT-L/16, ViT-L/32) [14], and Wide ResNet-50-2 [68].



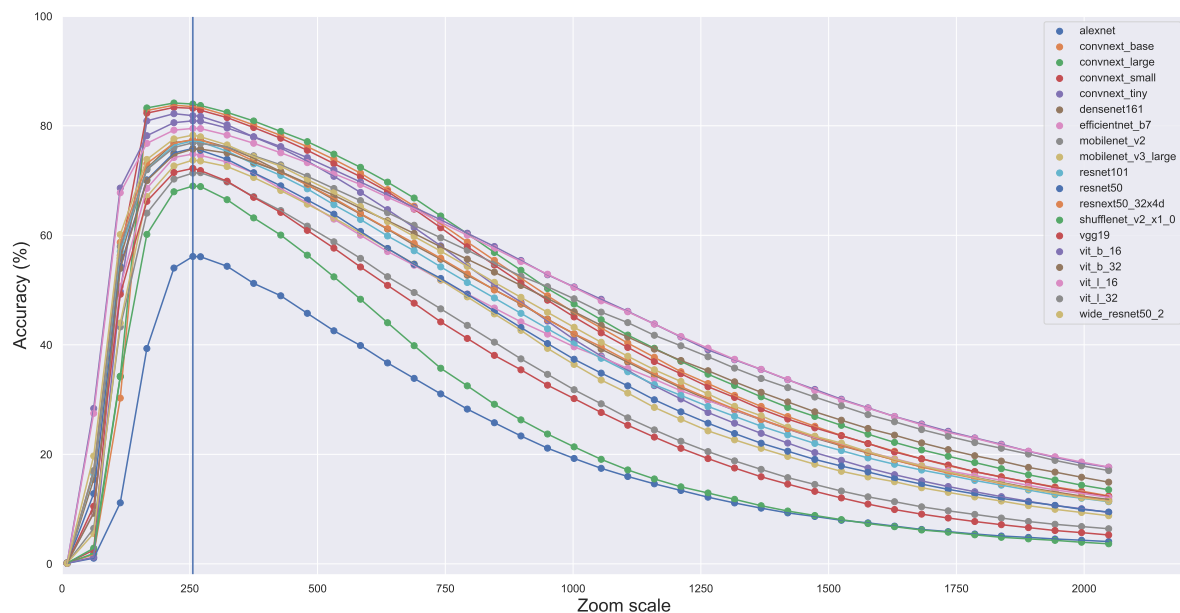


Figure A10: ImageNet accuracy using a 1-crop transform (the vertical line represents the standard ImageNet transform scale factor).

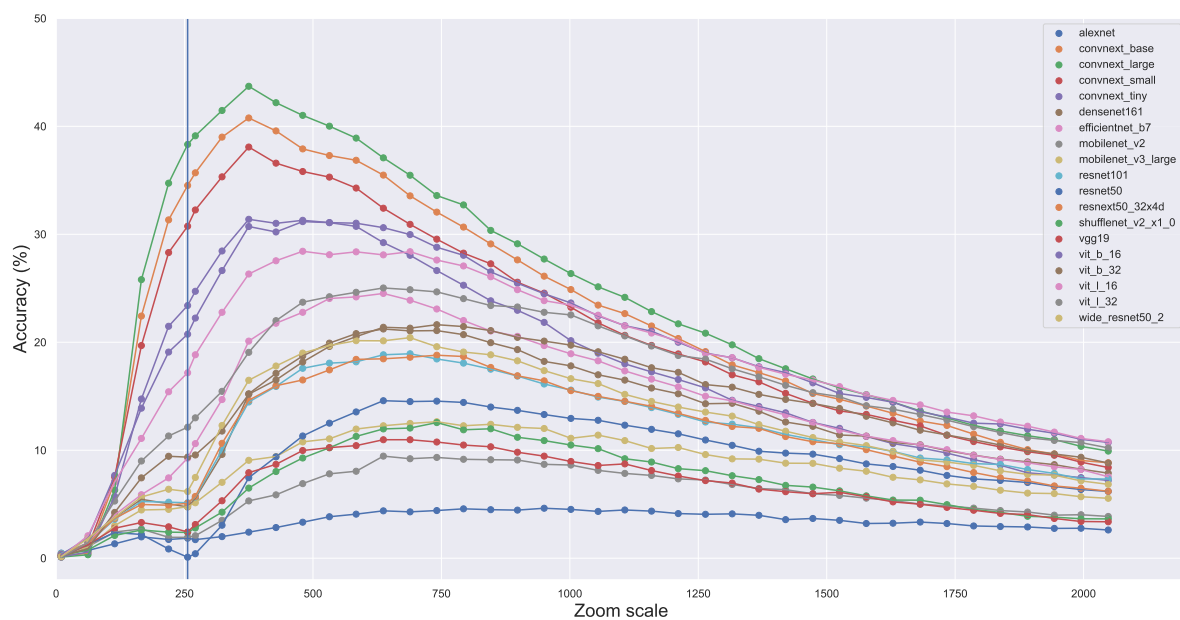


Figure A11: ImageNet-A accuracy using a 1-crop transform (the vertical line represents the standard ImageNet transform scale factor).

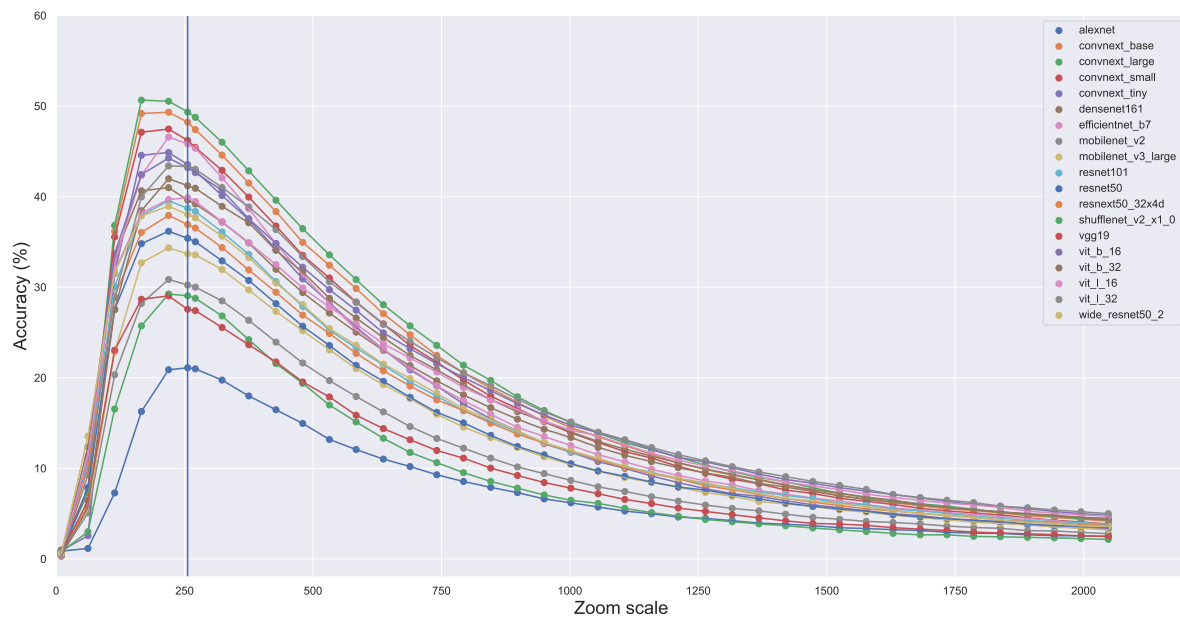


Figure A12: ImageNet-R accuracy using a 1-crop transform (the vertical line represents the standard ImageNet transform scale factor).

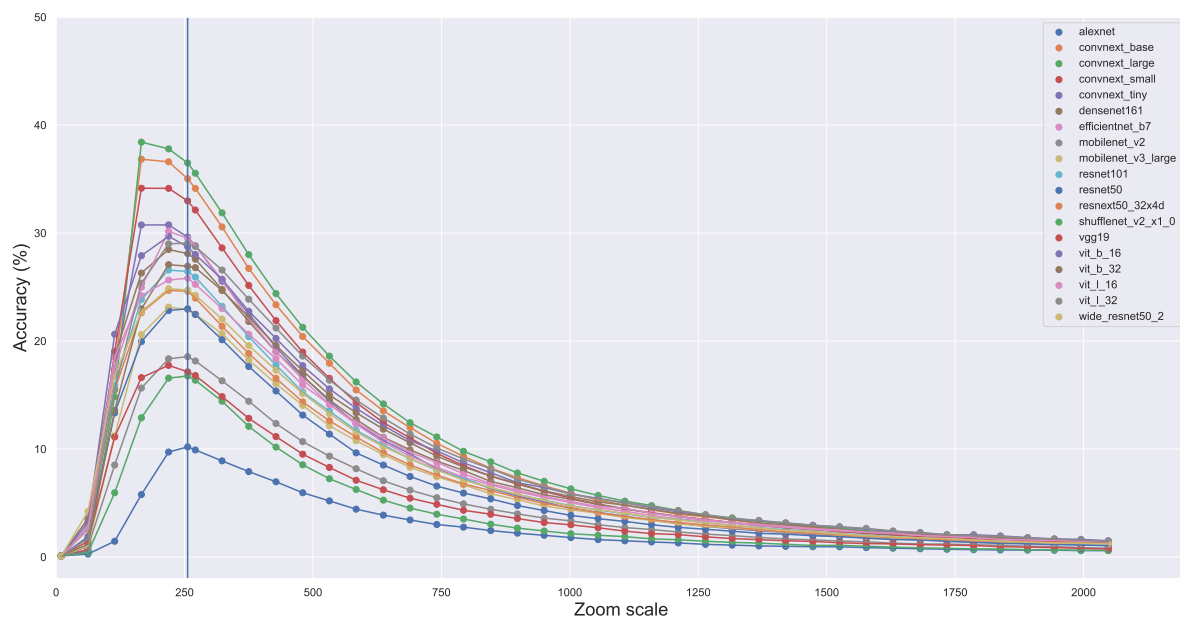


Figure A13: ImageNet-Sketch accuracy using a 1-crop transform (the vertical line represents the standard ImageNet transform scale factor).

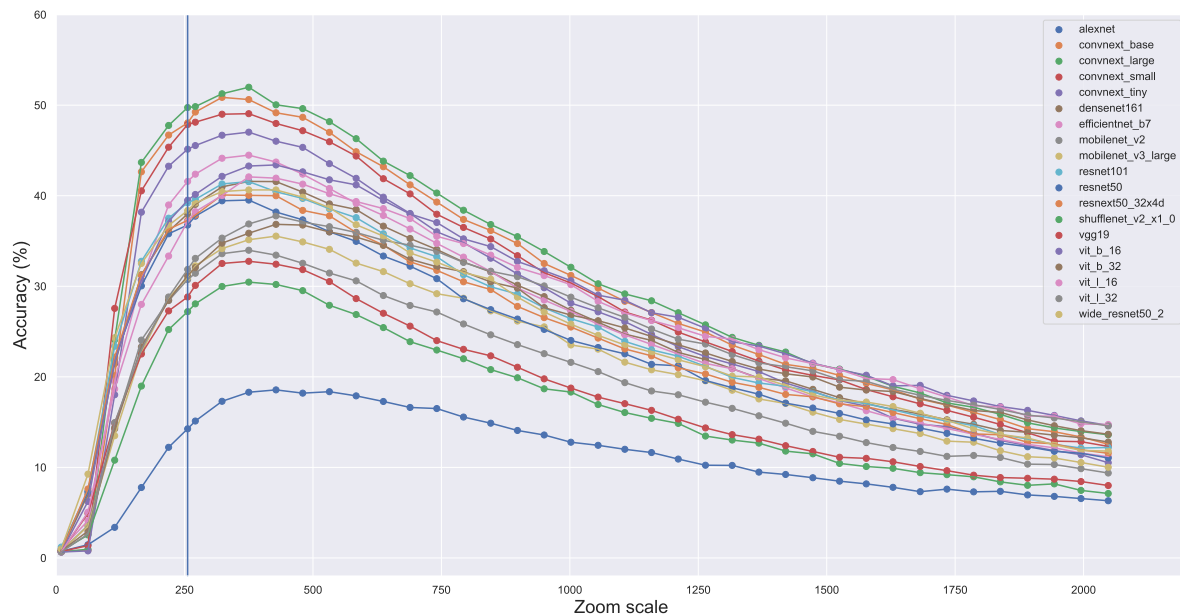


Figure A14: Accuracy using a 1-crop transform on 5K random images of the ObjectNet dataset (the vertical line represents the standard ImageNet transform scale factor).

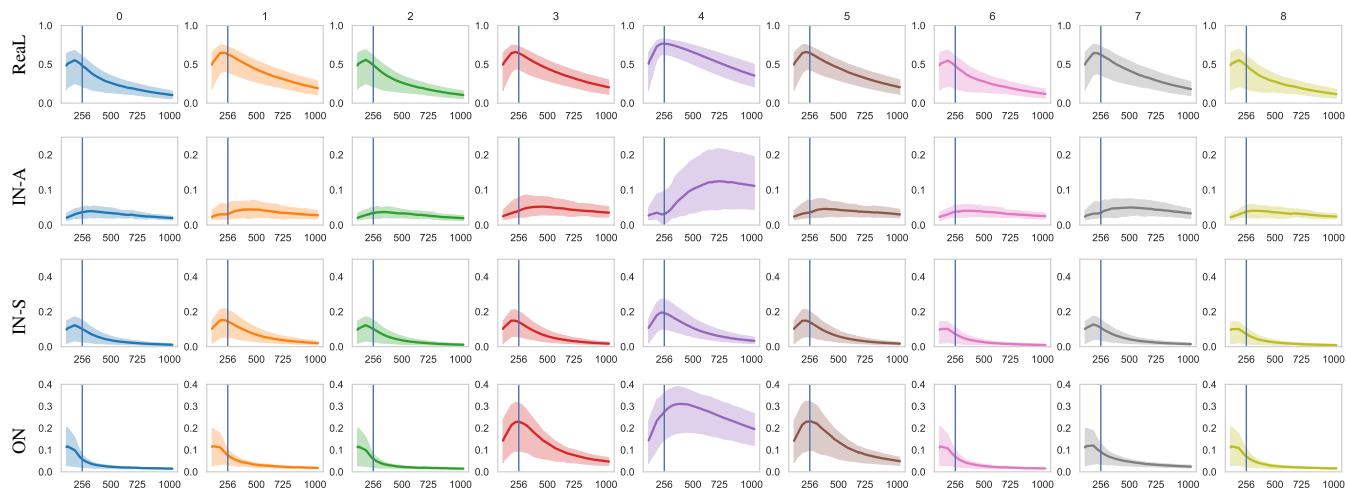


Figure A15: Breakdown of the accuracy of IN-trained models at different crop locations and scale size – Analysis of accuracy across various crop locations and scale sizes reveals that different datasets exhibit distinct optimal conditions. For instance, the IN-A dataset experiences a considerable increase in accuracy when zoomed in, while ImageNet-R yields better results when zoomed out.

### B.7. Background occlusion in ImageNet dataset



Figure A16: A sample image of the Tank class without occlusion (**left**) and with heavy background occlusion (**right**).

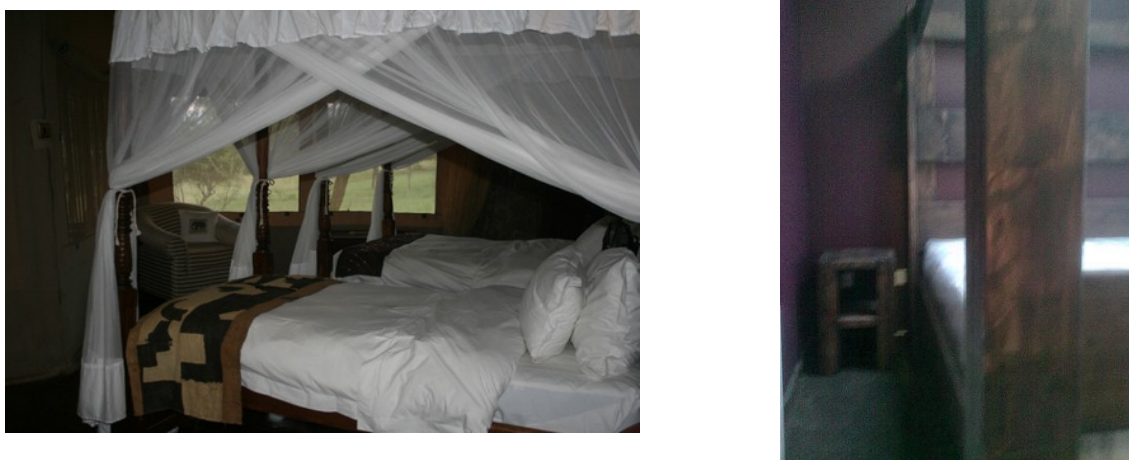


Figure A17: A clean sample image of the Four Poster class (**left**) and a low quality image with background occlusion (**right**).



## B.8. Hard ImageNet-Real samples

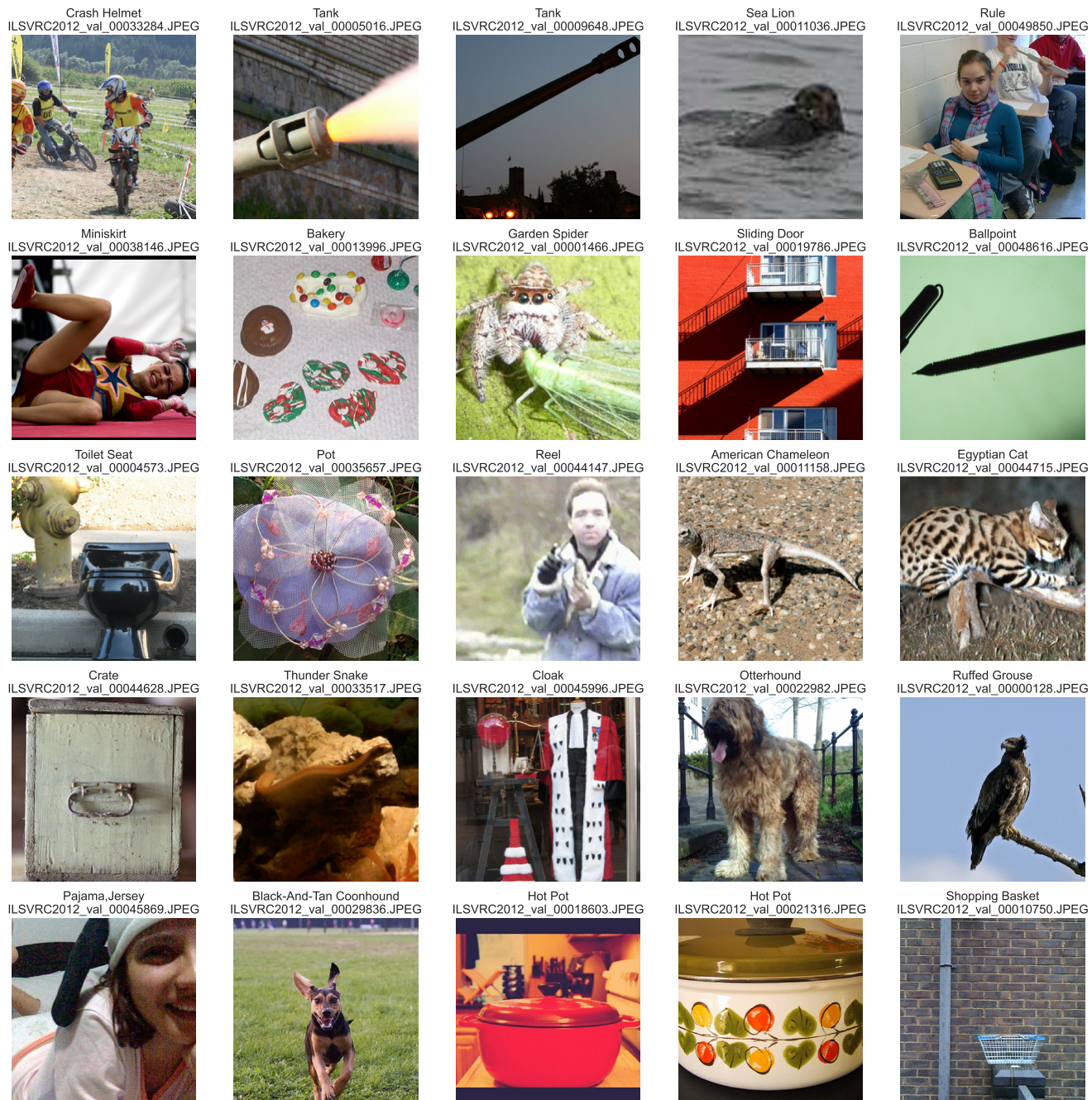


Figure A18: Hard ImageNet-Real samples

## C. Additional Experiments

In this section, we provide additional experiments with the proposed zoom-based transform.

### C.1. Zooming is similarly important to the foreground and background contents

Background pixels, despite often being neglected in image classification, can contain predictive signals [16, 46, 65, 72]. It has remained largely unknown how much the image context (background) could contribute to the model performance. While Zhu et al. [72] disentangle the predictiveness of background (BG) and foreground (FG) via model training, we directly measure how pretrained models perceive these two signals.

**Experiment** Using bounding-box annotations provided by Russakovsky et al. [48], we create two dataset variations of ImageNet: *FGSet* and *BGSet*, following Zhu et al. [72]. We mask all the background for *FGSet* as in Fig. A19b, and for *BGSet* we mask all the main objects, as depicted in Fig. A19d & Fig. A19f. After that, we compute the accuracy of these two sets with all tested classifiers using ImageNet and ImageNet-ReaL labels as in Tab. A5.

**Results** Our results suggest that zooming is important to ImageNet regardless of whether foreground or background features are used, with the difference for *FGSet* and *BGSet* on average being similar (Tab. A5). Additionally, when only the background features were available, almost half of ImageNet images (45.23%) could be correctly classified if optimal Zoom was used. Finally, we found that with only foreground information, ViT-B/32 could achieve a maximum possible accuracy of 95.50% given an optimal zooming method, suggesting that only  $98.75\% - 95.50\% = 3.25\%$  of images (Tab. 1) required the background information. These findings suggest that both foreground and background features are important for ImageNet classification, but that an optimal zooming method can considerably improve performance even in the absence of one of these feature sets.

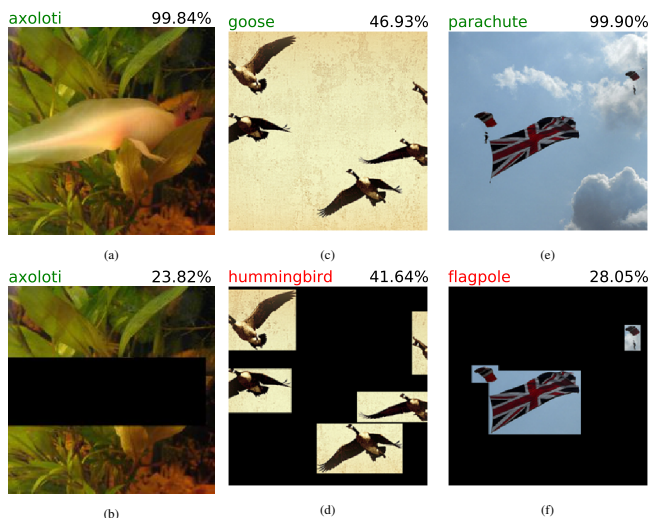


Figure A19: The foreground and the background both contain predictive signals. A ResNet-50 classifier can detect `axoloti` (a), even when the main object is masked (b). Removing the background from images of ‘goose’ (c) and ‘parachute’ (e) causes misclassification (d, f).

### C.2. Adversarial datasets contain more objects compared to ImageNet

So far, our findings indicate that if we apply the zoom-in operation to the two datasets of ImageNet-A and ObjectNet, the performance of conventional vision models improves consistently up to a certain threshold (Sec. 4 and Sec. 4.5). This suggests that the initial images contain distracting elements that impede the model from correctly identifying the object of interest. Both ImageNet-A and ObjectNet are considered out-of-distribution datasets, which are specifically designed to evaluate a vision model’s ability to withstand natural adversarial and pose attacks. We hypothesize that the primary reason that these datasets are hard can be attributed to background clutter, multiple objects, and the presence of a positional bias in these images.

Table A5: ImageNet classification from object-only and background-only signals. Numbers show the maximum possible top-1 accuracy (%) using zoom-based transforms for minimum set covers in Sec. 4.2. We discover that background signals potentially hold significance for image classification. The bold numbers show the highest possible accuracy per dataset and group.

	1-crop				Max possible using zooming			
	FGSet		BGSet		FGSet		BGSet	
	IN	ReaL	IN	ReaL	IN	ReaL	IN	ReaL
ResNet-18	59.77	64.97	4.91	7.84	89.89	92.04	25.81	31.33
ResNet-50	68.02	72.90	6.18	9.83	93.45	94.89	30.30	35.98
ViT-B/32	67.46	71.78	<b>9.72</b>	13.38	94.40	95.50	<b>39.70</b>	<b>45.23</b>
VGG-16	63.78	69.09	5.36	8.59	91.01	92.91	26.98	32.62
AlexNet	42.38	46.54	3.66	5.46	80.20	83.25	22.02	27.04
CLIP-ViT-L/14	<b>74.46</b>	<b>78.62</b>	9.49	<b>13.80</b>	<b>96.14</b>	<b>97.35</b>	36.85	42.51
mean	62.65	67.32	6.55	9.82	90.85	92.66	30.28	35.79

**Experiment** We use OWL-ViT [41], an open vocabulary object detection model, to quantify the number of objects present in three datasets of ImageNet, ImageNet-A, and ObjecNet. The OWL-ViT expects an input image with a set of object names and will determine if any object instances are present in the image. To specify object names, we use LVIS vocabulary [19], which encompasses a comprehensive list of 1203 distinct objects. The OWL-ViT model includes a threshold parameter that reflects its confidence level in its predictions. To assess whether different threshold values would affect our results, we conducted our experiment using both 0.1 and 0.05 as threshold values.

After calculating the distribution of the number of objects in images, we perform a Mann-Whitney U test to determine whether there is a statistically significant difference in this distribution between datasets. As each dataset has a different number of classes, we limited our analysis to shared classes between any two datasets.

**Results** The results of our study reveal a contrast between ImageNet and ImageNet-A, as well as ImageNet and ObjectNet. This finding implies a dissimilarity between the images in the original ImageNet dataset and its OOD datasets that might arise from the presence of background clutter. Specifically, on average, images in ImageNet-A and ObjectNet datasets tend to feature more objects, which can pose more significant distractions for image classification models.

The results of the Mann-Whitney U test also reflect this finding, the p-value for both thresholds was found to be less than 0.05, which is statistically significant at the 95% confidence level (Tab. A6).

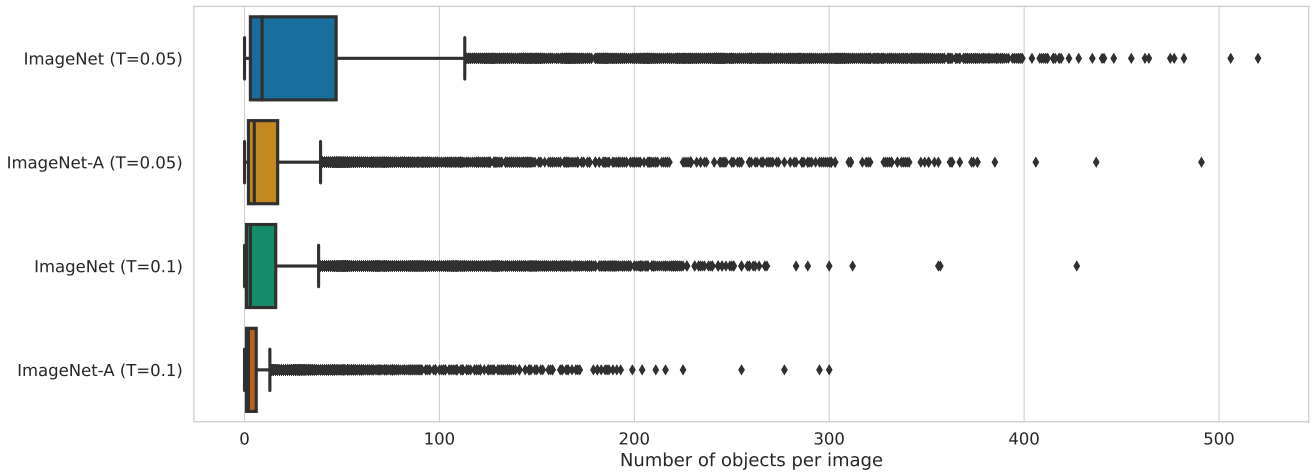


Figure A20: Comparison of the number of objects in two datasets of ImageNet and ImageNet-A using OWL-ViT [41] –  $T$  denotes the classification’s threshold

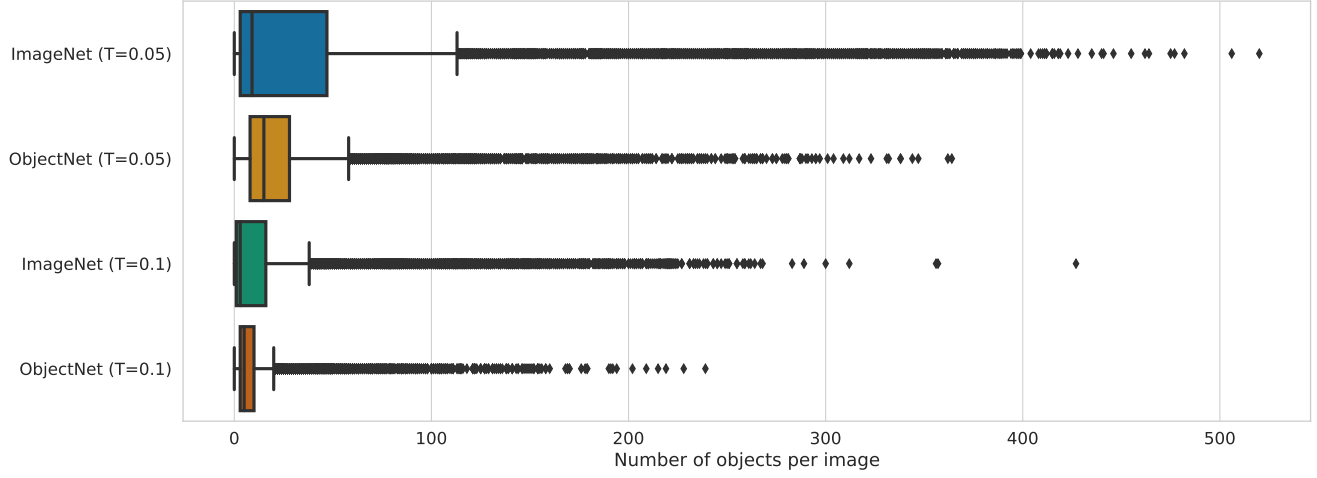


Figure A21: Comparison of the number of objects in two datasets of ImageNet and ObjectNet using OWL-ViT [41] –  $T$  denotes the classification’s threshold

### C.2.1 $p$ -values for Mann Whitney U test

Table A6: The result of the Mann-Whitney U test to compare ImageNet with ImageNet-A and ObjectNet

	$T = 0.05$	$T = 0.01$
<b>ImageNet-A</b>	6.27E-265	1.71E-235
<b>ObjectNet</b>	1.80E-02	3.66E-02



### C.3. Zooming further improves robustified models on ImageNet-A

Intensive data augmentations have been proven to significantly boost CNNs’ performance [55,64] on ImageNet. Motivated by these previous successes and the fact that neural networks trained on diverse augmentations are able to learn robust representations [34], we want to know if robustified pretrained models (*i.e.* trained with intensive augmentations) could reach higher accuracy on ImageNet-A using zooming in.

**Experiment** We test 4 different ResNet-50 classifier versions that have been trained with different data augmentation procedures. From the the `torchvision` library, we select two sets of model weights; trained with (V2<sup>3</sup>) and without (V1<sup>4</sup>) data augmentations. We also take two other models trained with DeepAugmentation+AugMix [21] and MoEx+CutMix [33]. The second column in Tab. A7 represents the accuracy of models using 1-crop.

**Results** Zooming in consistently helps ResNet-50 networks, with improvements varying from +13 to +24 points. The best-performing network is `torchvision-V2` which uses the max aggregator and achieves 29.65%. These results suggest that simple aggregation over the proposed zoom transform is effective for datasets that have dominant center bias.

Table A7: The results of different aggregation functions on four ResNet-50 variants when tested on ImageNet-A (%). Each model has been trained using different training-time augmentation techniques. Improvements values in parentheses are with respect to the 1-crop baseline.

ResNet-50	Baseline	Max	Mean
<code>torchvision V1</code>	0.21	16.11 (+15.90)	6.23
<code>MoEx+CutMix [33]</code>	8.60	24.72 (+16.12)	15.32
<code>DeepAug+AugMix [21]</code>	3.94	27.93 (+23.99)	13.16
<code>torchvision V2</code>	16.62	29.65 (+13.03)	22.08

---

<sup>3</sup>`ResNet50_Weights.IMAGENET1K_V2`

<sup>4</sup>`ResNet50_Weights.IMAGENET1K_V1`

## D. Visualization

In this section, we provide several visualizations of zooming transforms.

### D.1. Visualizations for 36 top performing zoom transforms



Figure A22: Different framing of an image of a `lorikeet` according to 36 high-performing transforms of a ResNet-50 model



Figure A23: Different framing of an image of a lorikeet according to 36 high-performing transforms of a ViT/B-32 model



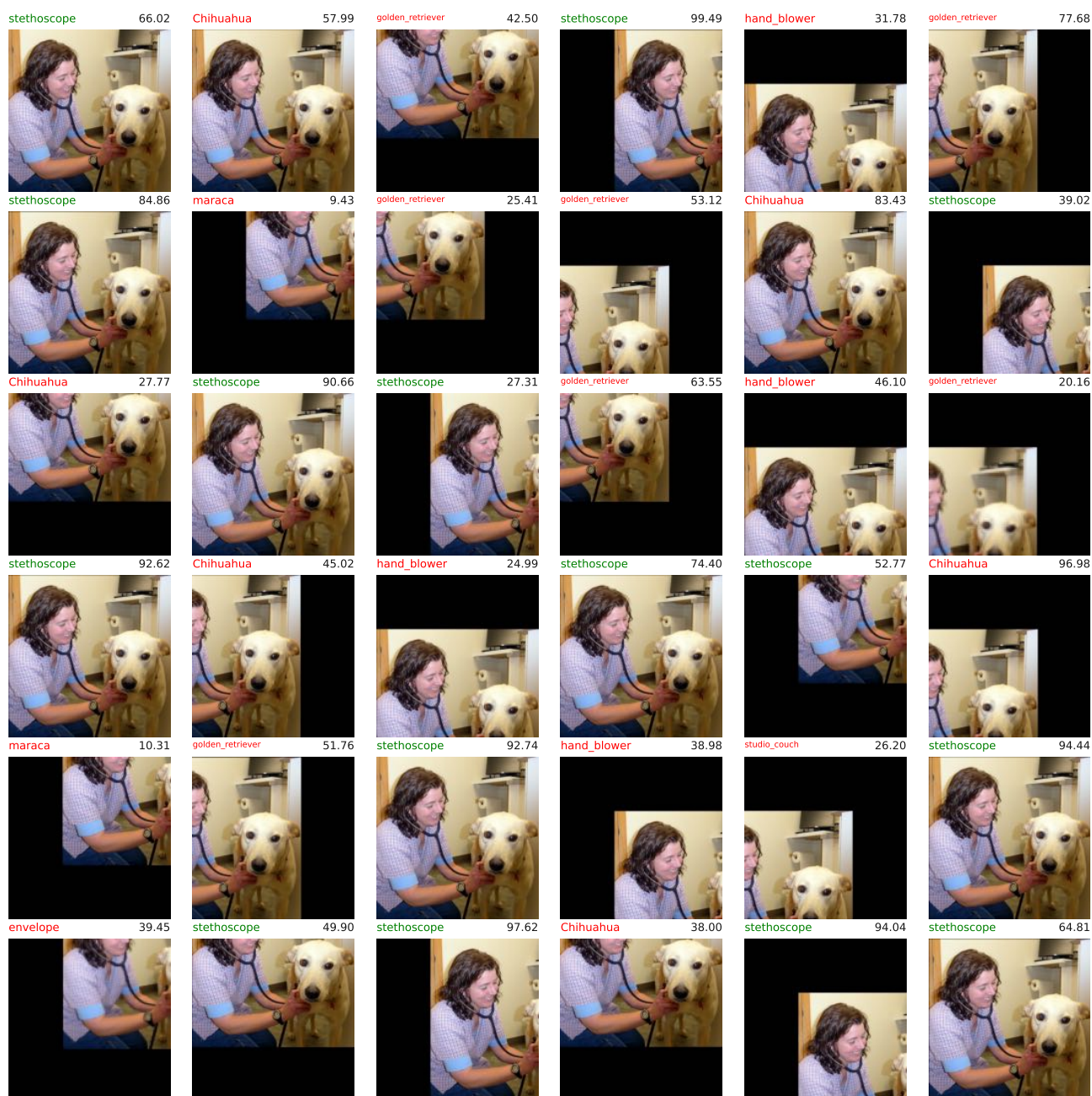


Figure A24: Different framing of an image of a stethoscope according to 36 high-performing transforms of a ResNet-50 model

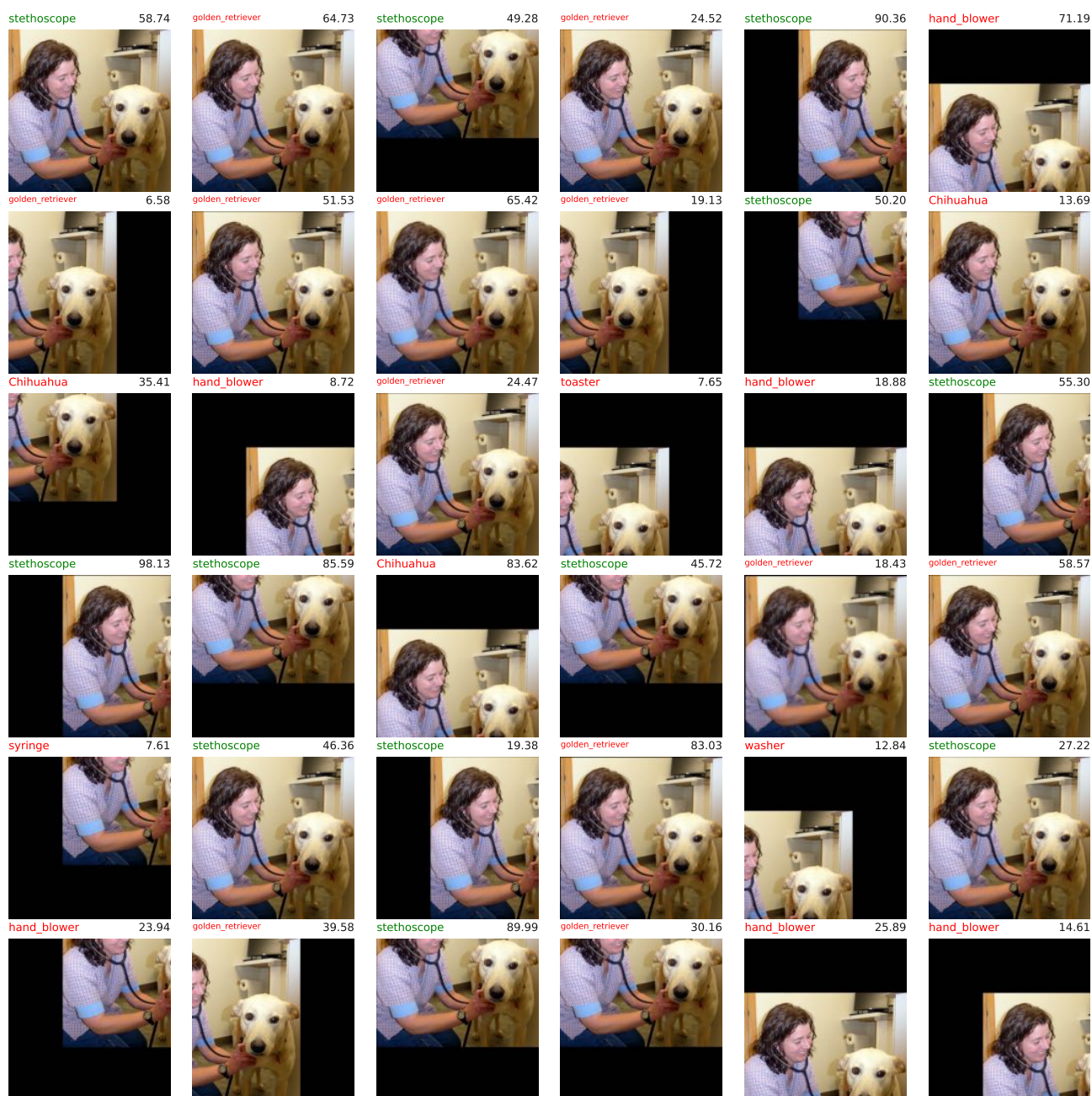


Figure A25: Different framing of an image of a stethoscope according to 36 high-performing transforms of a ViT/B-32 model



## D.2. Overview of 324 transforms

The visualizations below illustrate the transforms that result in the correct prediction of the query image, using ViT-B/32 [14] and CLIP-ViT-L/14 [44]. Each circle represents a transform, with the initial zoom scale indicated in the accompanying text. The green circles represent the transformations that lead to correct classification, while the red circles indicate incorrect ones.



Figure A26: Visualization of effective transforms that lead to the correct classification of an image containing `scorpion`, using a ViT-B/32 model.



Figure A27: Visualization of effective transforms that lead to the correct classification of an image containing `scorpion`, using a CLIP-ViT-L/14 model.



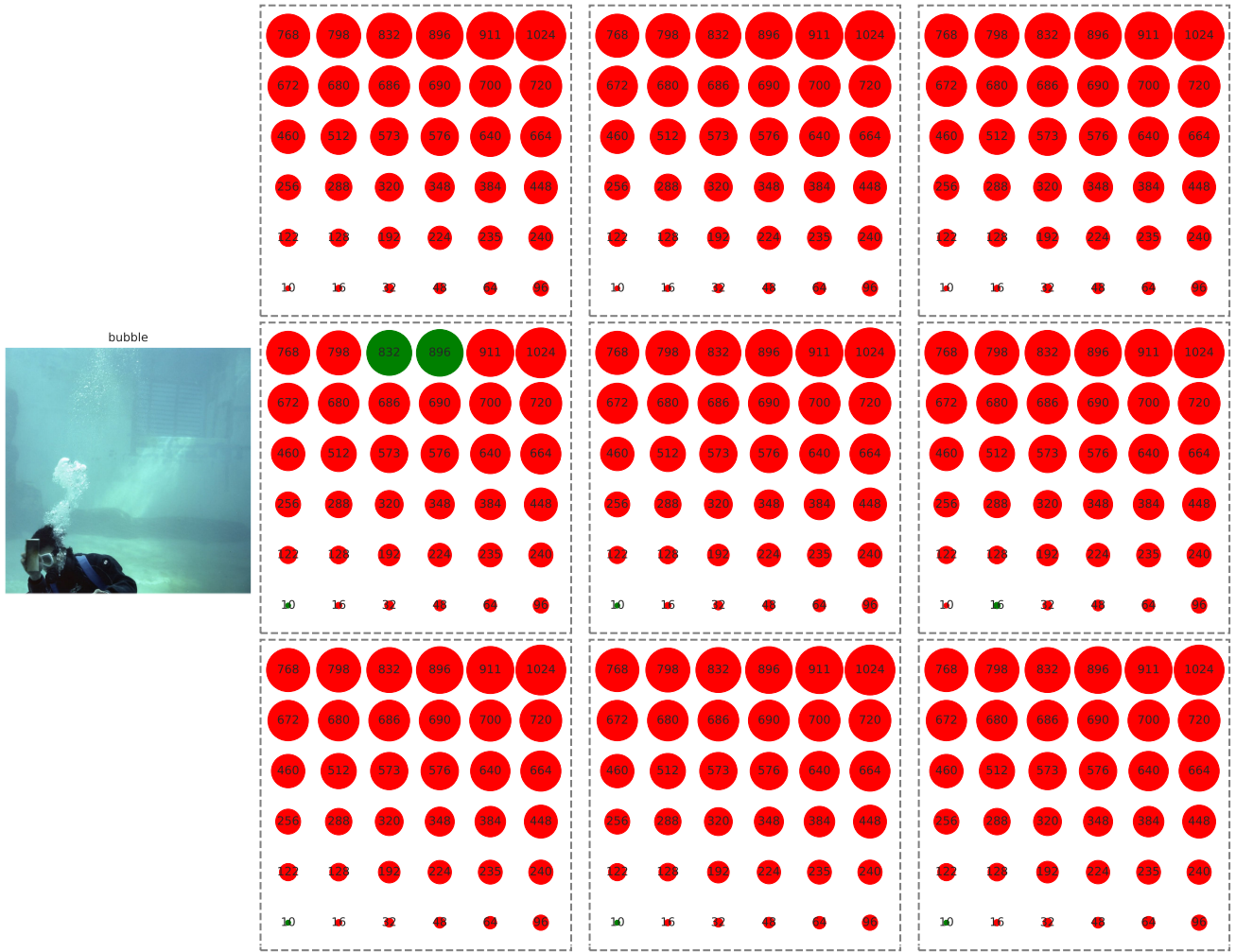


Figure A29: Visualization of effective transforms that lead to the correct classification of an image containing bubble, using a CLIP-ViT-L/14 model.

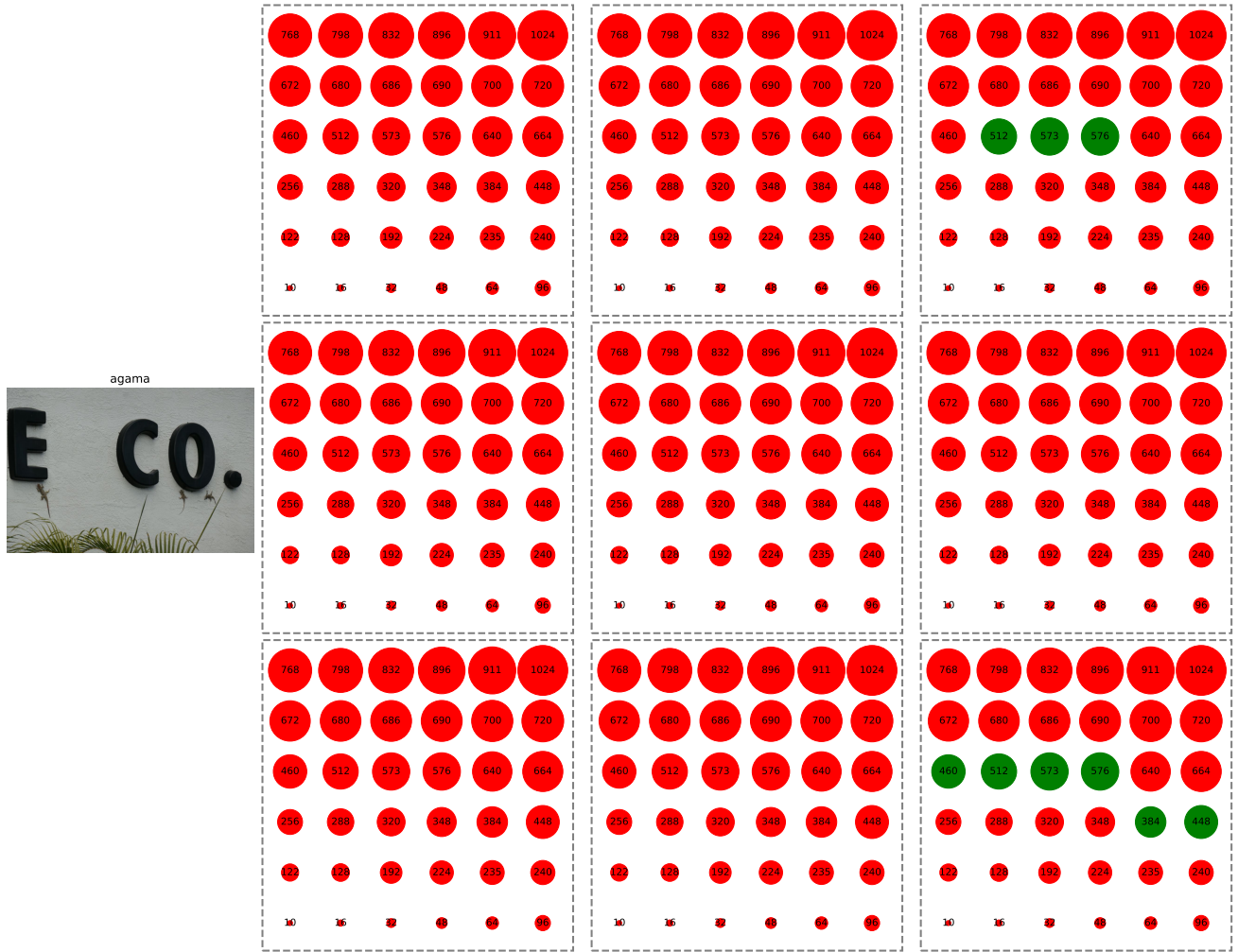


Figure A30: Visualization of effective transforms that lead to the correct classification of an image containing agama, using a ViT-B/32 model.



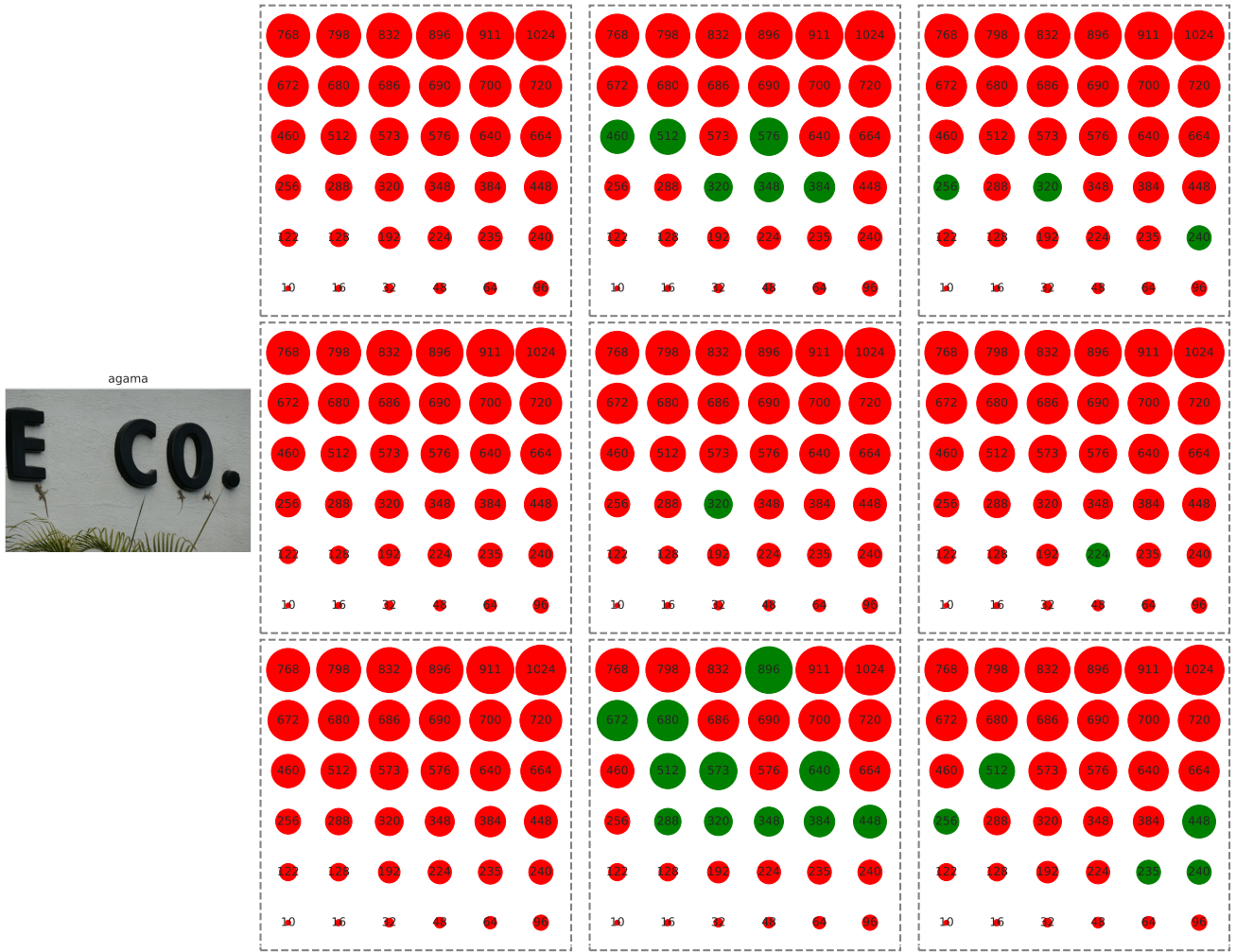


Figure A31: Visualization of effective transforms that lead to the correct classification of an image containing *agama*, using a CLIP-ViT-L/14 model.

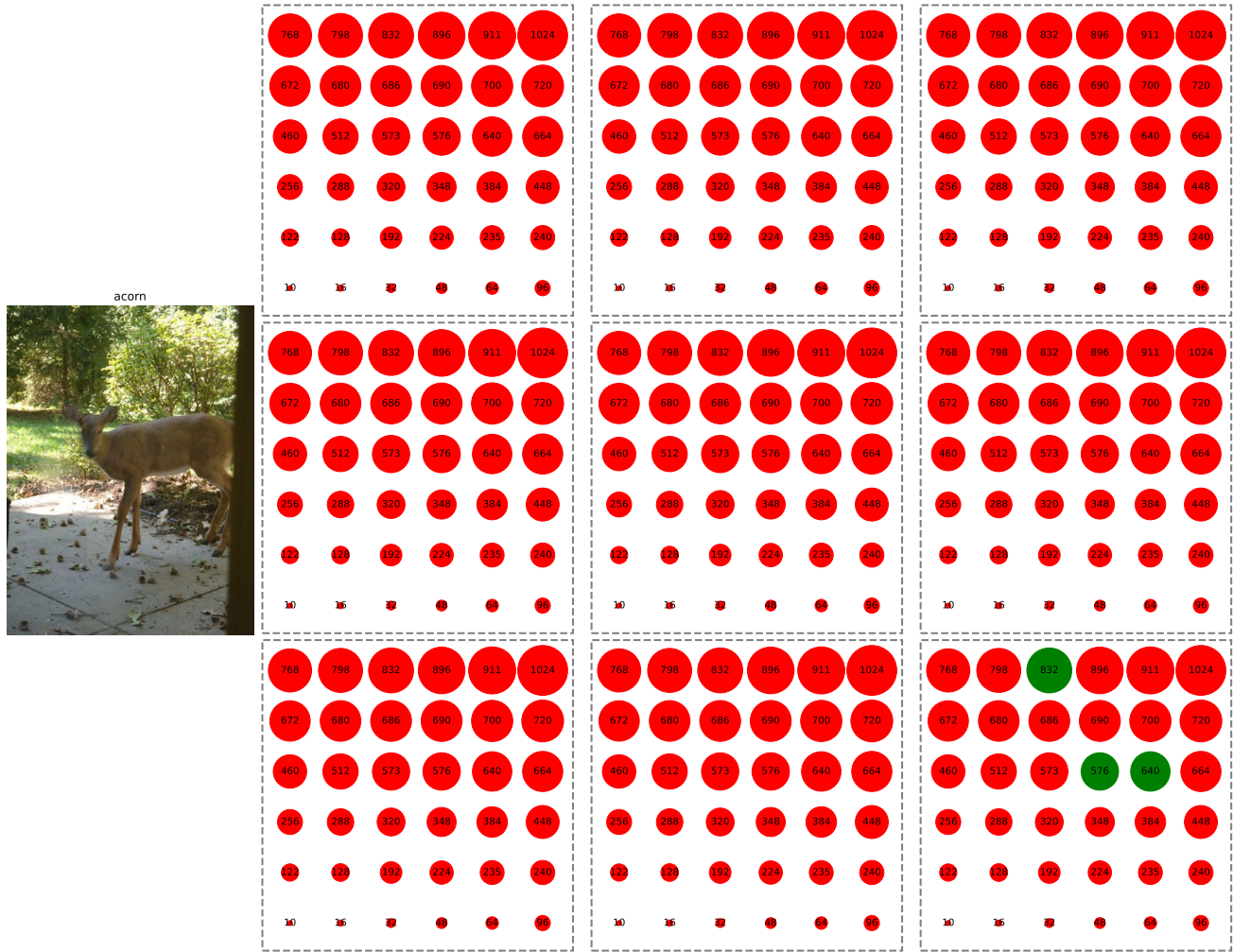


Figure A32: Visualization of effective transforms that lead to the correct classification of an image containing `acorn`, using a ViT-B/32 model.

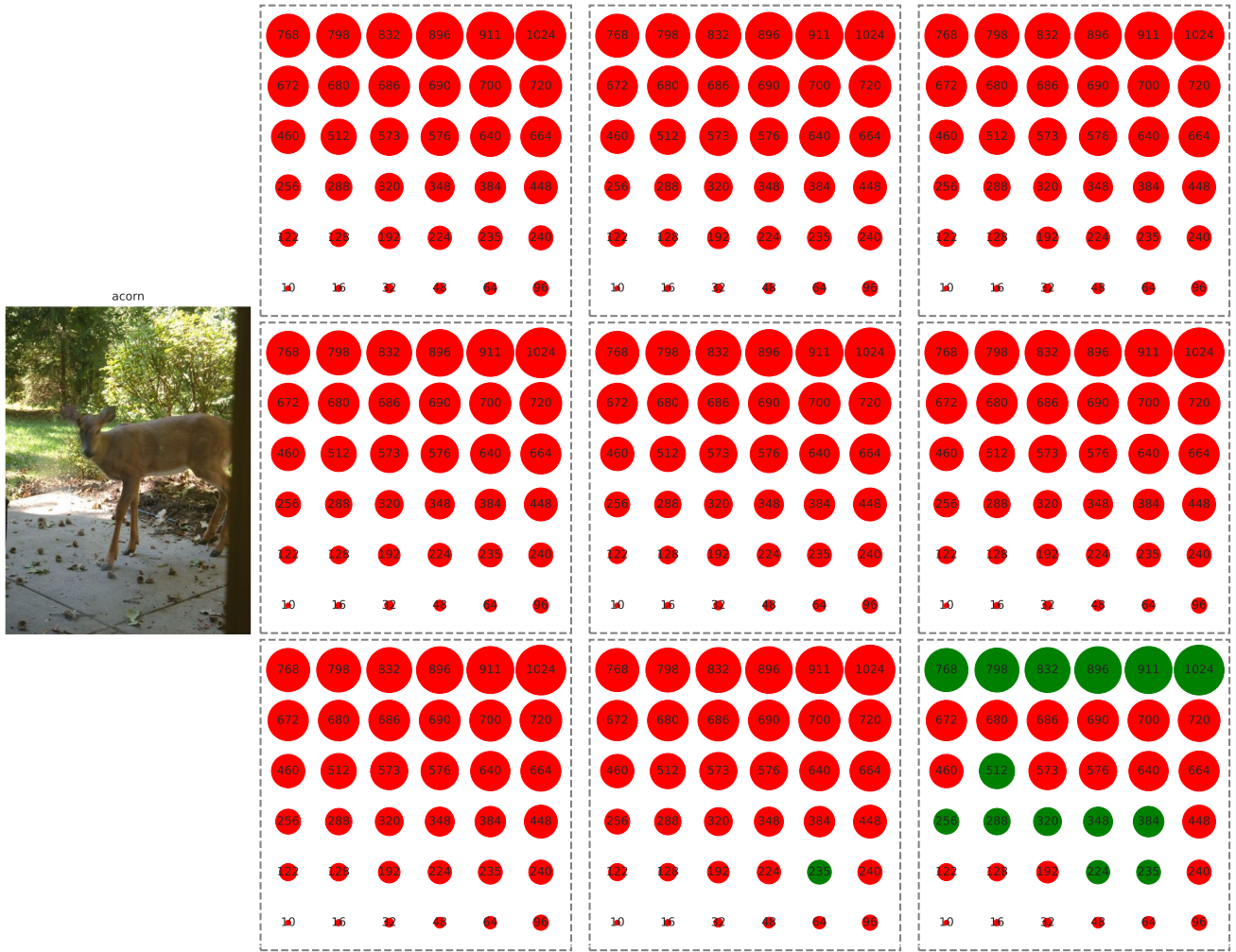


Figure A33: Visualization of effective transforms that lead to the correct classification of an image containing `acorn`, using a CLIP-ViT-L/14 model.

### D.3. Only *zoom-out* solves

Sample images that required zooming out to be classified correctly.

#### D.3.1 ImageNet-Sketch

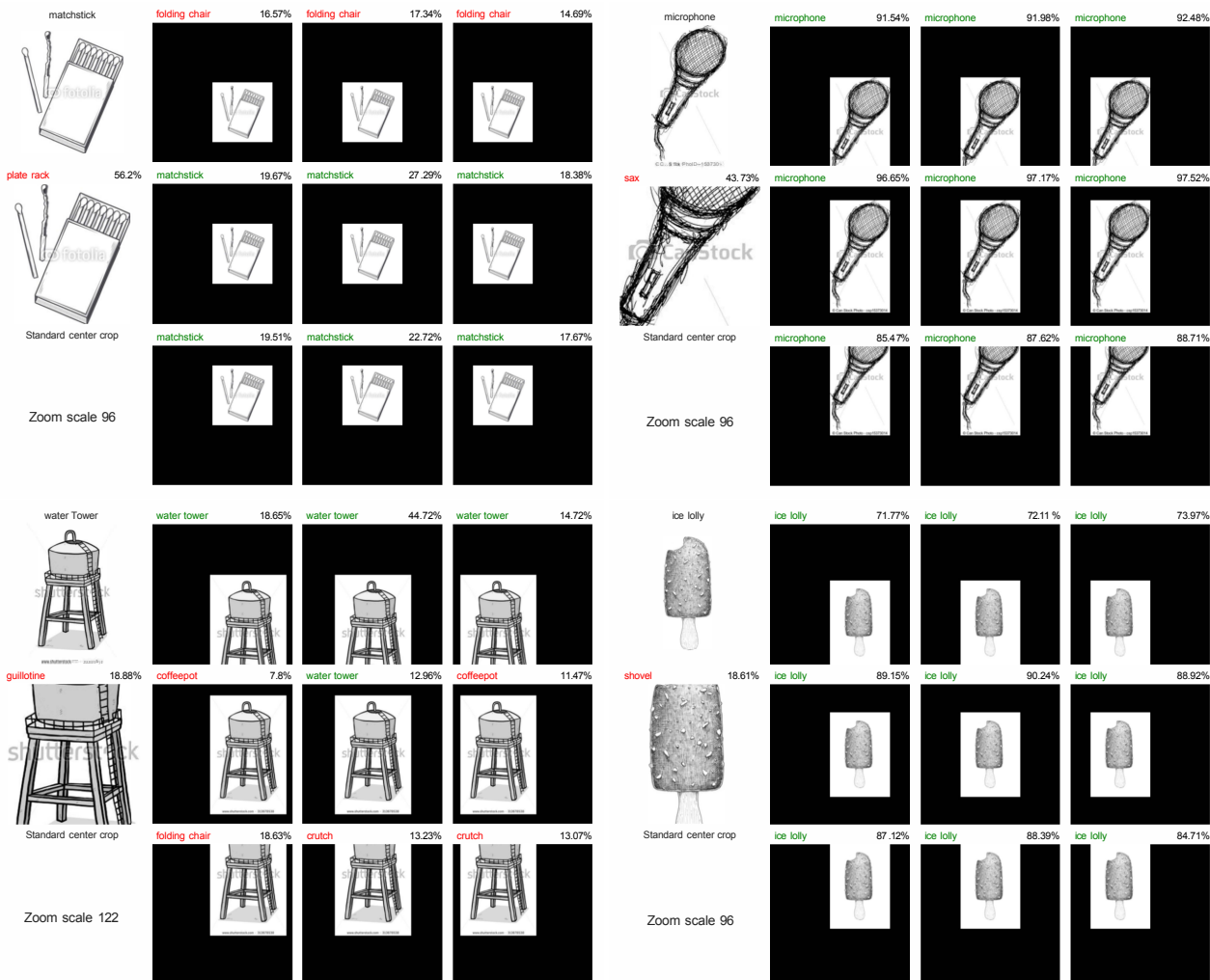


Figure A34: ImageNet-Sketch images that can only be solved using *zoom-out*. Predictions are from a ResNet-50 classifier.

### D.3.2 ImageNet-R

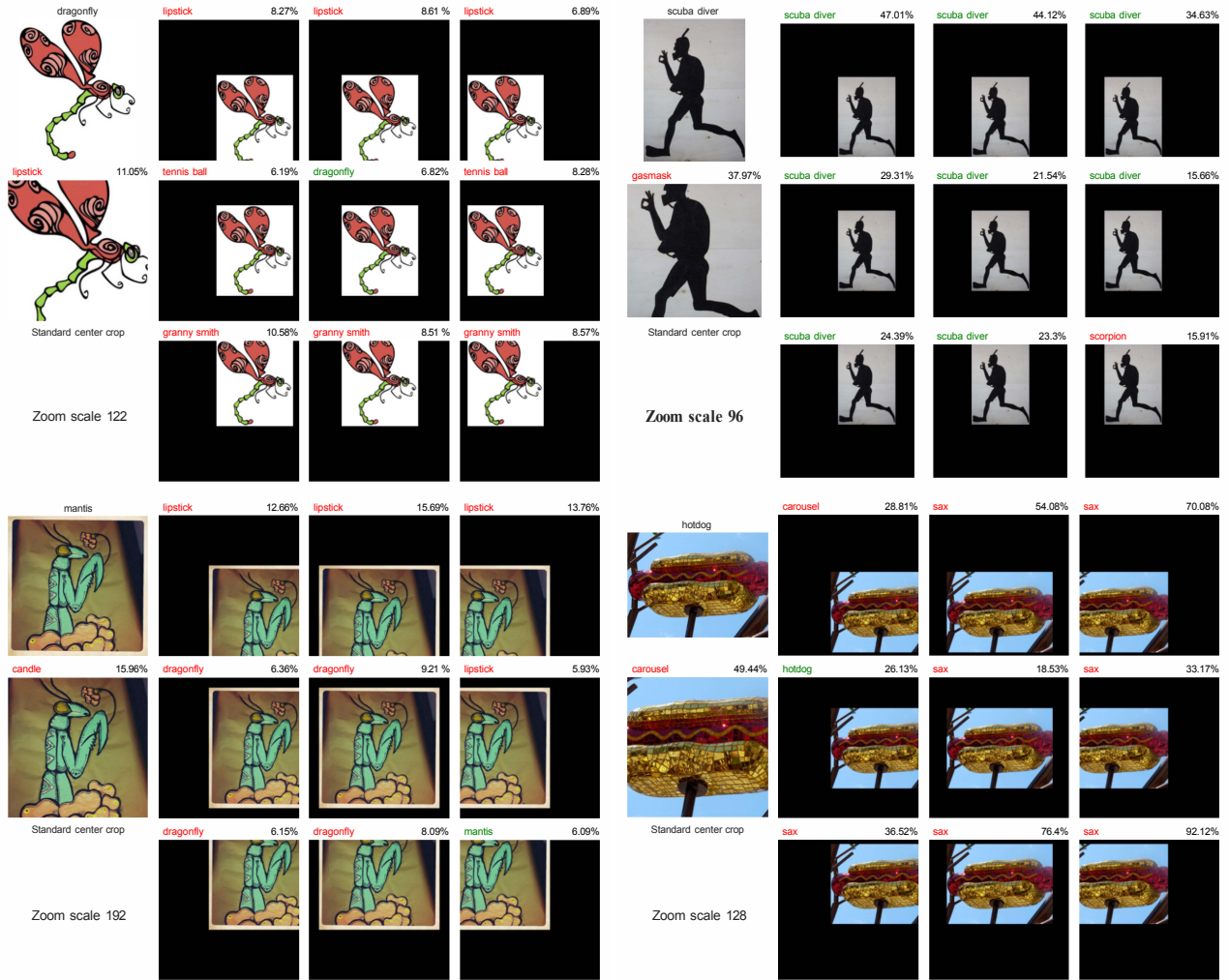


Figure A35: ImageNet-R images that can only be solved using *zoom-out*. Predictions are from a ResNet-50 classifier.



### D.3.3 ObjectNet

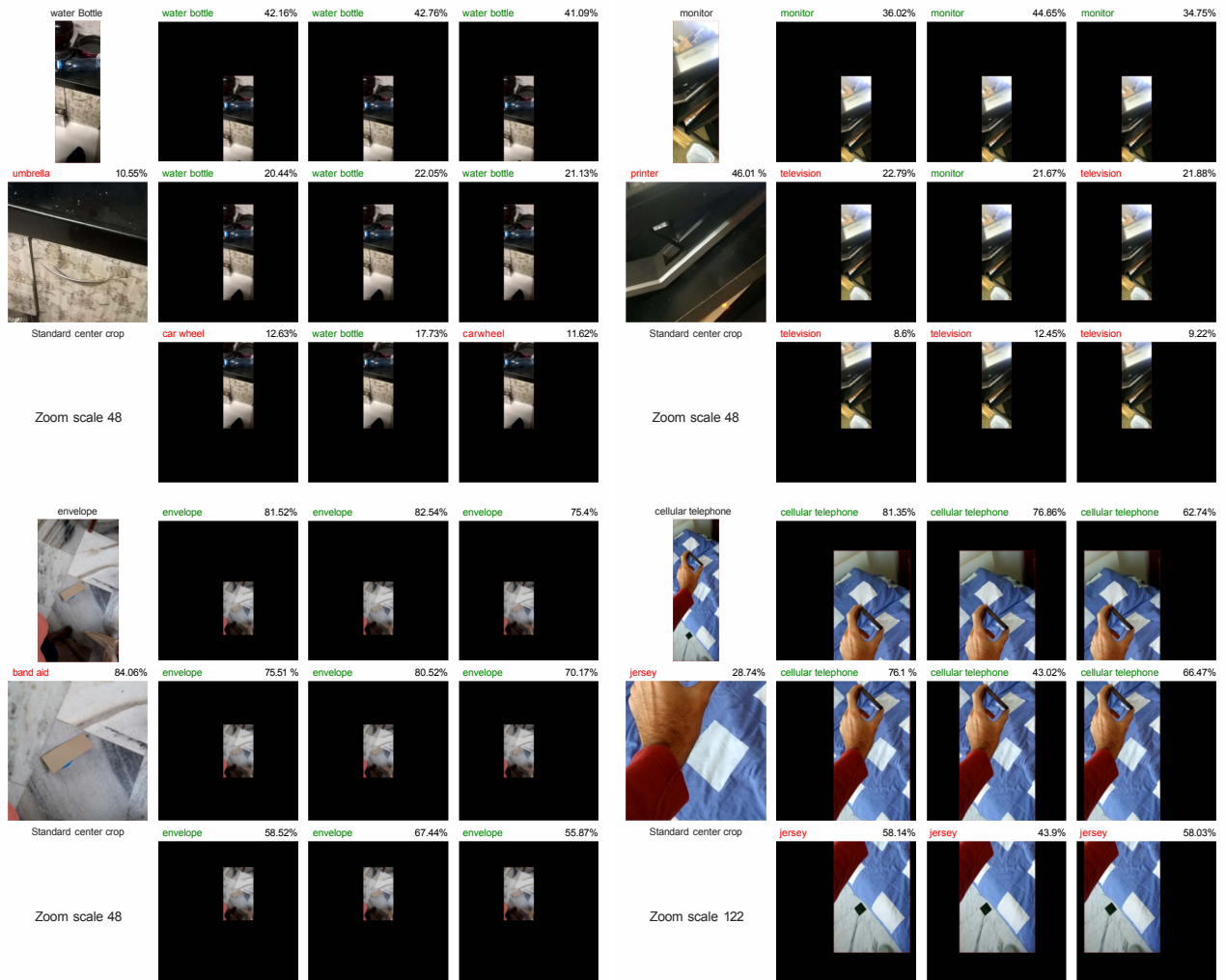


Figure A36: ObjectNet images that can only be solved using *zoom-out*. Predictions are from a ResNet-50 classifier.

## D.4. Only *zoom-in* solves

Sample images that required zooming in to be classified correctly.

### D.4.1 ObjectNet

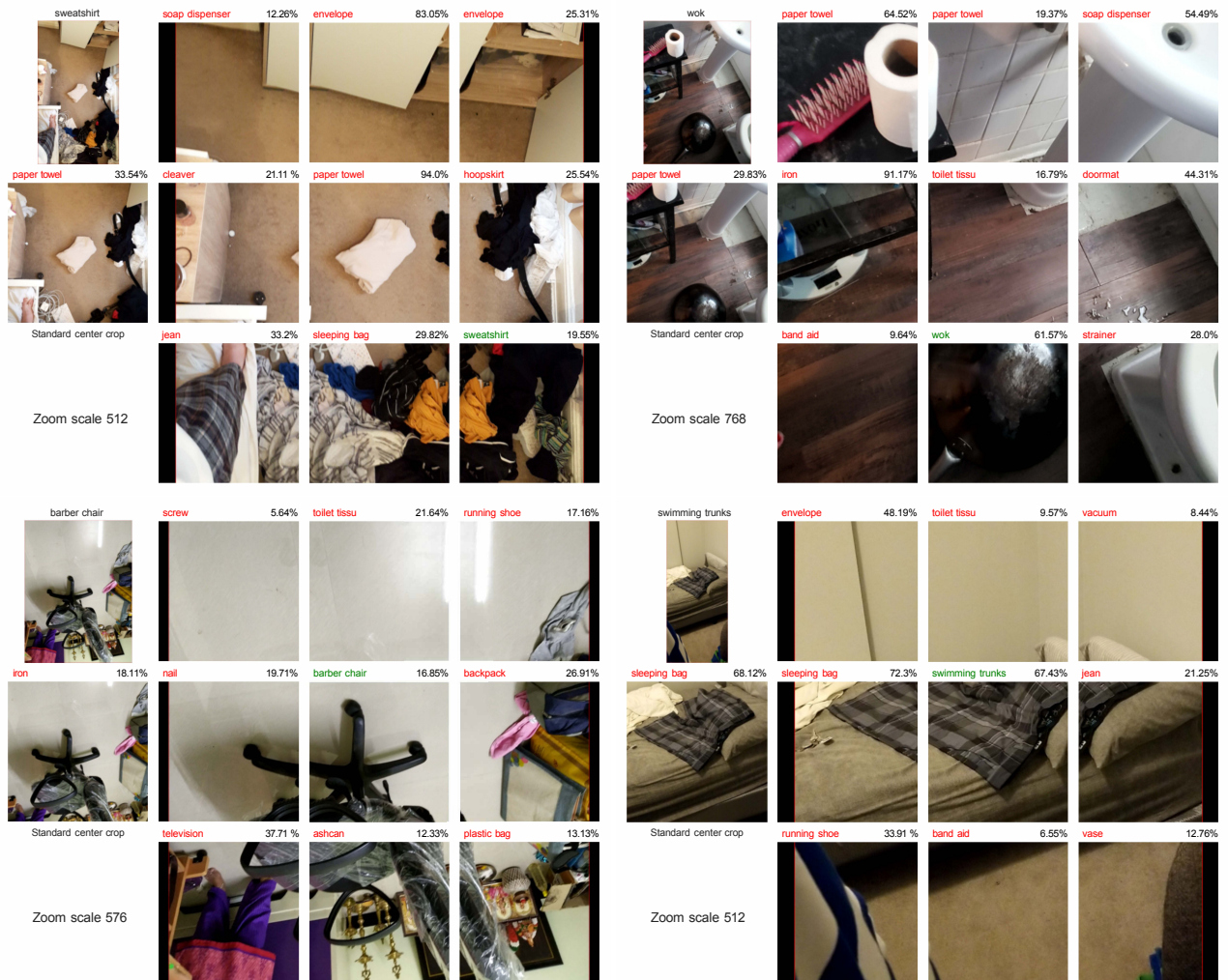


Figure A37: ObjectNet images that can only be solved using *zoom-in*. Predictions are from a ResNet-50 classifier.



## D.5. AugMix and RandomResizedCrop



Figure A38:  $K = 16$  sample outputs from AugMix [23] (which yields the results of random sampling from 13 transformations that include both spatial and color distortions).



Figure A39:  $K = 16$  sample outputs from RandomResizedCrop (RRC), which basically randomly zooms into an arbitrary region in the input image.



Figure A40:  $K = 16$  sample outputs from AugMix [23] (which yields the results of random sampling from 13 transformations that include both spatial and color distortions).



Figure A41:  $K = 16$  sample outputs from RandomResizedCrop (RRC), which basically randomly zooms into an arbitrary region in the input image.

E. ImageNet-Hard

In this section, we provide details about the distribution of the dataset used in the ImageNet-hard dataset.

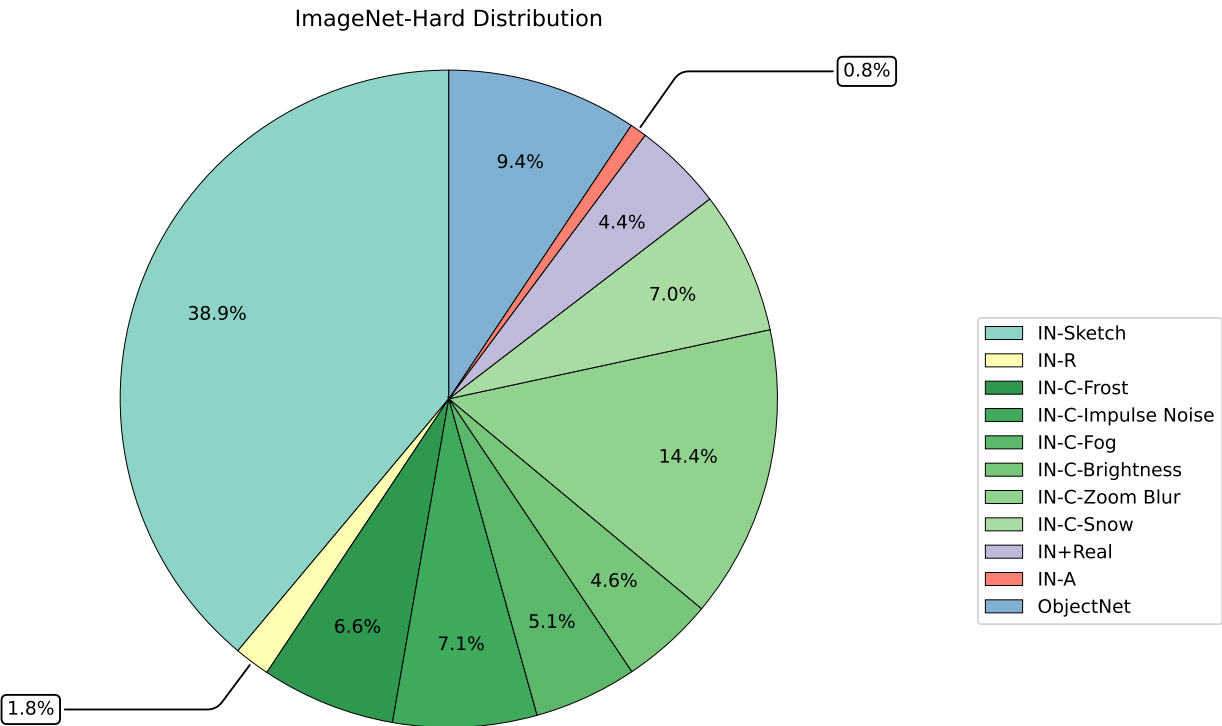


Figure A42: The distribution of the dataset within the ImageNet-Hard Dataset.